JBC Papers in Press. Published on November 9, 2015 as Manuscript M115.691519
The latest version is at http://www.jbc.org/cgi/doi/10.1074/jbc.M115.691519

Molecular mechanism responsible for fibronectin-controlled alterations in tissue stiffness in advanced chronic liver fibrogenesis

Ayumi Iwasaki[1,7#], Keiko Sakai[1,2#], Kei Moriya[2#], Takako Sasaki[3], Douglas R. Keene[4], Riaz Akhtar[5], Takayoshi Miyazono[6], Satoshi Yasumura[6], Masatoshi Watanabe[7], Shin Morishita[8], and Takao Sakai[1,2]

[1]MRC Centre for Drug Safety Science, Department of Molecular and Clinical Pharmacology, Institute of Translational Medicine, University of Liverpool, Liverpool L69 3GE, UK;
[2]Department of Biomedical Engineering, Lerner Research Institute, Cleveland Clinic, Cleveland, OH 44195, USA;
[3]Department of Biochemistry, Faculty of Medicine, Oita University, Oita, 879-5593, Japan;
[4]Micro-Imaging Center, Shriners Hospital for Children, Portland, OR 97231, USA;
[5]Centre for Materials and Structures, School of Engineering, University of Liverpool, Liverpool L69 3GH, UK;
[6]Department of Gastroenterology and Hepatology, and Transfusion Medicine and Cell Therapy, Toyama University, Toyama 930-0194, Japan;
Graduate School of [7]Biomedical Engineering and [8]Environmental and Information Science, Yokohama National University, Yokohama 240-8501, Japan.

#These authors contributed equally to this work

Running title: Tissue stiffness in advanced liver fibrosis

Key Words: extracellular matrix; fibronectin; tissue stiffness; lysyl oxidase; TGF-β; chronic hepatic fibrogenesis; mouse model of liver disease; conditional knockout mouse

Correspondence: Takao Sakai, M.D., Ph.D., MRC Centre for Drug Safety Science, Department of Molecular and Clinical Pharmacology, Institute of Translational Medicine, University of Liverpool, Sherrington Building, Ashton Street, Liverpool L69 3GE, United Kingdom.
TEL: 0151-795-2704; FAX: 0151-794-5540; Email: sakait@liverpool.ac.uk

Abstract

Fibrosis is characterized by extracellular matrix (ECM) remodeling and stiffening. However, the functional contribution of tissue stiffening to non-cancer pathogenesis remains largely unknown. Fibronectin (Fn) is an ECM glycoprotein substantially expressed during tissue repair. Here we show in advanced chronic liver fibrogenesis using a mouse model lacking Fn that, unexpectedly, Fn-null livers lead to more extensive liver cirrhosis, which is accompanied by increased liver tissue stiffness and deteriorated hepatic functions. Furthermore, Fn-null livers exhibit more myofibroblast phenotypes, and accumulate highly disorganized/diffuse collagenous ECM networks composed of thinner and significantly increased number of collagen fibrils during advanced chronic liver damage. Mechanistically, mutant livers show elevated local TGF-β activity and lysyl oxidase expressions. A significant amount of active lysyl oxidase is released in Fn-null hepatic stellate cells in response to TGF-β1 through canonical and non-canonical Smad such as PI3 kinase-mediated pathways. TGF-β1-induced collagen fibril stiffness in Fn-null hepatic stellate cells is significantly higher compared to wild-type cells. Inhibition of lysyl oxidase significantly reduces collagen fibril stiffness, and treatment of Fn recovers collagen fibril stiffness to wild-type levels. Thus, our findings indicate an indispensable role for Fn in chronic liver fibrosis/cirrshosis in negatively regulating TGF-β bioavailability, which in turn modulates ECM remodeling and stiffening, and consequently preserves adult organ functions. Furthermore, this regulatory mechanism by Fn could be translated for a potential therapeutic target in broader variety of chronic fibrotic diseases.

Introduction

Fibrosis is a part of the wound-healing response that maintains organ structure and integrity following tissue damage. However excessive fibrosis contributes to a number of diseases such as liver

fibrosis (1). Liver fibrosis is defined as an abnormal response of the liver to persistent injury and affects tens of millions of people worldwide (2). It is caused by hepatotropic virus infection, drug and alcohol abuse. Liver fibrosis is of great clinical importance since normal liver architecture is disrupted and liver function is ultimately impaired. There is no effective treatment for liver fibrosis and many patients end up with a progressive form of the disease, liver cirrhosis, often requiring a liver transplant (3,4). The hallmark of liver fibrosis is excessive accumulation of mainly type I collagen-containing extracellular matrices (ECMs), and therefore involves both wound healing and fibrotic processes. ECM production and remodeling in the liver following injury involves the activation of specific cell types, hepatic stellate cells, which transdifferentiate into contractile and proliferative myofibroblasts (5-7).

Collagen is the most abundant scaffolding ECM in tissue/organ stroma and contributes significantly to tissue/organ integrity (8). The Lysyl oxidase (LOX) family enzymes are copper-dependent amine oxidases that catalyze the process of covalent crosslinking of collagen by oxidatively deaminating specific lysine and hydroxylysine residues in the telopeptide domains, which increases collagen stiffness (9,10). Collagen crosslinking stiffens the ECM and has been implicated in cancer cell invasion (11). Collagen crosslinking also accompanies tissue fibrosis mediated by several profibrogenic cytokines (12). However, the functional contribution of collagen crosslinking to non-cancer pathogenesis remains largely unknown.

Transforming growth factor (TGF)-β is a profibrogenic master cytokine responsible for promoting differentiation of tissue-resident fibroblasts into myofibroblasts, upregulation of ECM production including fibronectin (Fn), and downregulation of ECM degradation (13). Growing evidence suggests a mechanism by which Fn plays a role in TGF-β signaling (14). Fn is involved in the initial incorporation of latent TGF-β-binding protein (LTBP)-1 into the ECM *in vitro* (15). TGF-β is secreted in a biologically inactive (latent) form in a complex (large latent complex [LLC]) with TGF-β latency associated protein (LAP) and LTBPs (16). The extracellular TGF-β activity in response to injury is regulated by the local activation of latent TGF-β complex to active TGF-β. Indeed, elevated TGF-β bioavailability is frequently observed in chronic fibrotic diseases, and the inhibition of local TGF-β activation can protect against the progression of fibrosis in several adult chronic fibrotic diseases (17-20). In spite of numerous *in vitro* studies and animal models, TGF-β/Fn interdependence in the fibrogenic response to advanced chronic liver damage has not yet been addressed *in vivo*.

Fn is a large dimeric glycoprotein that exists in blood plasma in its soluble form (plasma type) and in its insoluble form (cellular type) as a part of the ECM of almost every tissue in an organism. Plasma Fn is produced solely by hepatocytes in the liver (21,22). Extensive *in vitro* functional studies have indicated that Fn plays a key role in a wide range of cellular behaviors (21,22), and prominent expression of Fn is observed in response to liver injury (23). Based on *in vitro* findings, it has been postulated that collagen network formation depends on the Fn matrix (24,25). We therefore hypothesized that removal of Fn from the *in vivo* system could prevent extensive ECM network formation following tissue damage. To define the functional identity of Fn in adult tissue remodeling, we recently established a null-condition for both Fn isoforms in adult liver. We demonstrated a Fn-independent mechanism of collagen fibrillogenesis and identified TGF-β-signaling and type V collagen as essential elements for collagen fibrillogenesis in response to liver injury (26). However, it remains unknown whether the extent of the initial Fn deposition could contribute to the critical turning point from normal to abnormal healing during the development of chronic tissue fibrosis. Furthermore, it is also unclear how ECM remodeling by myofibroblasts results in changes in mechanical tension and supports the activation of pathogenic signaling pathways. Here, we have addressed the molecular mechanism responsible for tissue stiffness in advanced chronic liver fibrogenesis using a mouse model lacking both Fn isoforms in the adult liver.

Experimental Procedures

Maintenance of mice

Mice lacking both plasma and cellular type fibronectin in the liver (liver Fn-null mice) were generated by intraperitoneal injections of polyinosinic-polycytidic acid (pI-pC) in the Fn(fl/fl)/*Mx-Cre+* strain as described previously (26). Fn-null livers showed normal liver morphology, and no obvious inflammation or fibrosis was noted after pI-pC injections (26). All mice were maintained and bred at the animal facility in the Cleveland Clinic, OH, USA, and the University of Liverpool, Liverpool, UK, in accordance with institutional guidelines. Mice were regularly

monitored and had free access to standard mouse chow and water. Mice received humane care in accordance with institutional guidelines.

Induction of chronic liver injury by carbon tetrachloride (CCl_4)

Chronic liver injury was induced intraperitoneally by administrations of CCl_4 solution in olive oil (Fluka) (0.5 ml/kg body weight as 50% [vol/vol], twice a week for up to 17 weeks) in sex-matched, 12- to 15-week-old mice (26,27). Control and liver Fn-null mice were derived from the same litters. Mice injected only with olive oil as negative controls showed no phenotypes (data not shown).

Antibodies, cytokines and reagents

The following antibodies were used for the analyses: rabbit polyclonal antibody (pAb) against mouse fibronectin (Chemicon); rabbit mAb (E184, Epitomics) against αSMA; rabbit pAb against pSmad3 which specifically recognizes the phosphorylated C-terminal serine 423/425 of Smad3 (also cross-reacted with phosphorylated C-terminal serine 465/467 of Smad2) (a kind gift from Dr. Koichi Matsuzaki, Kansai Medical University, Osaka, Japan); rabbit pAb against LOX (Sigma-Aldrich); rabbit pAb against cleaved caspase3 (Cell Signaling); mouse mAb against HSC70 (Santa Cruz); mouse mAb against β-actin (clone AC15, Sigma); affinity-purified rabbit pAbs against mouse LAP of TGF-β1, mouse LTBP-3, human LTBP-4, and human type V collagen (26). The preparation and characterization of rabbit pAbs against bovine type I collagen and type III procollagen have been described elsewhere (28). Rabbit pAb against human lysyl oxidase was generated using its protein residue #22-168 expressed in HEK293 cells as an antigen and affinity purified as described (29). Rabbit pAb against LTBP-1 was a kind gift from Dr. Lynn Sakai (Research Center, Shriners Hospitals for Children, Portland, OR, USA). FITC- and Cy3-conjugated donkey anti-rabbit IgG, and peroxidase-conjugated donkey anti-mouse and anti-rabbit IgG were from Jackson ImmunoRes Lab. 4'6-diamidino-2-phenylindole (DAPI) was from Molecular Probes. Envision™+ System-HRP labeled polymer was from DAKO. Recombinant human TGF-β1 was from R&D Systems. Bovine plasma fibronectin was from Sigma. All inhibitors were from Calbiochem.

Histological analysis, immunohistochemistry and immunofluorescence, and transmission electron microscopy

For histological analysis, liver samples were either directly frozen in OCT compound (Tissue-Tek, Sakura Finetek) or fixed overnight in 4% paraformaldehyde in PBS, pH 7.2, and dehydrated in a graded alcohol series before being embedded in paraffin. Sirius Red staining was performed according to standard protocols. Immunohistochemistry and immunofluorescence studies were performed as described previously (30,31). Double-immunohistochemical analysis with paraffin-embedded tissue sections was performed as described (26). Briefly, after the first antigen-antibody reaction, the slides were incubated with dissociation buffer containing 0.1 M Glycine-HCl (pH 2.2) to dissociate immunoglobulins from antigenic sites. Then the second antigen-antibody reaction was subsequently performed. We carried out the second reaction without antibodies and confirmed the complete dissociation of the first immunoglobulins.

For quantification of fibrotic areas in response to chronic liver injury and LOX signal intensity in hepatic stellate cells, images were captured with the same gain, offset, magnitude and exposure time. A minimum of 5 different images were randomly selected, and intensities were quantified using ImageJ software (version 1.48, US National Institutes of Health). For cellular signal intensity, the mean intensity in each cell (intensities/areas, 50 cells) was measured and the average intensity per cell (relative fluorescent units) was calculated as described elsewhere (32).

Transmission electron microscopy (TEM) was performed as described previously (26).

Polarization microscopy analysis

Quantitative polarization microscopic analysis was performed on Sirius red stained sections using Abrio™ LS PolScope (CRI Inc., Woburn, MA) (33). In PolScope images, the brightness of each pixel is strictly proportional to birefringence "retardance" of the particular object point and independent of its slow axis orientation (34). Measured retardances and orientations are represented as pseudo-colors. Images make it possible to determine specimen anisotropy (retardance and azimuth) at all angles (360°) simultaneously, and permit quantitative measurements on the orientation and the degree of organization of the fibers (35). In the present analysis, any azimuth (slow axis orientation) was covered by a 180° range because a fiber bundle has no head or tail. Fiber retardations and orientations were assessed with an automated analyzing system. Fifty measurements were taken in each of the three

regions and averaged. The degree of fiber alignment is represented by a calculation of the angular deviation of each orientation distribution. Thus, the smaller the angular deviation, the more aligned the fibers are.

Atomic force microscopy (AFM) analysis

The nanomechanical properties of the liver sections were investigated with atomic force microscopy (AFM: NanoScope VIII MultiMode AFM, Bruker Nano Inc., Santa Barbara, CA). The AFM was equipped with a 150 × 150 × 5 μm scanner (J-scanner) operated with the Peakforce Quantitative Nanomechanical Mapping (PFQNM) modality. Liver samples were rapidly frozen in OCT compound (Tissue-Tek, Sakura Finetek) following which 10 μm thick sections were prepared using a cryostat (Leica CM1950, Leica Microsystems, UK) and adhered to glass slides coated with Vectabond (Vector Laboratories Ltd). Cells were directly seeded on glass coverslips and cultured for 7 days. Then the glass slides/cover slips were adhered to metal support stubs using adhesive pads, and the samples were imaged at ambient conditions using a silicon nitride tip. The tip had a nominal tip radius of 8 nm and a 5 N/m spring constant (Bruker TAP150A probe). The preparation method used for the AFM imaging maintained the tissue/cellular structure for imaging without the need for any chemical fixation. The PFQNM method was calibrated using a reference polymer (PS1, Vishay Measurements Group UK) with a known elastic modulus (2.8 ± 0.1 GPa). The spring constant and deflection sensitivity was calibrated using the reference sample and the same AFM probe was used for imaging every sample. The data were fitted with the Derjaguin–Muller–Toporov (DMT) model to extract the elastic modulus, as described previously (36). For tissue samples, 10 x 10 μm images were collected and the mean elastic modulus was determined using Bruker Nanoscope software, v 1.5. Each image had a resolution of 384 samples/line. The regions selected for AFM were guided by Sirius Red-stained images of serial sections. Smaller scans (2 x 2 μm) were conducted in collagen fibril-rich areas and used to determine the elastic modulus distribution pixel-by-pixel in these locations. A Gaussian fit was applied to the data. For cell culture samples, collagen fibril areas were selected from 5 x 5 μm scan images, and the mean elastic modulus for collagen fibrils were determined from 0.5 x 0.5 μm scans.

Real-time PCR

Real-time PCR was performed as described previously (37). The following primers were used:

ColIa1 forward, 5'-GGGCGAGTGCTGTGCTTT-3';
ColIa1 reverse, 5'-GGTCCCTCGACTCCTACATCTTC-3';
Col3a1 forward, 5'-CTGTAACATGGAAACTGGGGAAA-3';
Col3a1 reverse, 5'-CCATAGCTGAACTGAAAACCACC-3';
Col5a1 forward, 5'-GAGGACCACACAGGGAAGC-3';
Col5a1 reverse, 5'-CTTGTAGACACTGAGAGCAATTCG-3';
MMP8 forward, 5'-GGGATTATGGAAATGCCTCGAT-3';
MMP8 reverse, 5'-CTGTTTTCACTTCAGCCCTTGA-3';
MMP13 forward, 5'-CTTCTTCTTGTTGAGCTGGACTC-3';
MMP13 reverse, 5'-CTGTGGAGGTCACTGTAGACT-3';
LOX forward, 5'-CCTATGCGGCAGACATAGACT-3';
LOX reverse, 5'-CCAGGTAGCTGGGGTTTACA-3';
LOXL1 forward, 5'-ATGTGCAGCCTGGGAACTAC-3';
LOXL1 reverse, 5'-CACCACGTTGTTGGTGAAGT-3';
LOXL2 forward, 5'-CGTTGGAGTGGTGTGTAGTGAG-3';
LOXL2 reverse, 5'-CGAAAGGCAGAAAGGATGG-3';
LOXL3 forward, 5'-GCCACGTAGTCTGCGGTATG-3';
LOXL3 reverse, 5'-AGGGAGAGGTGGGCTTCTGT-3';
LOXL4 forward, 5'-GCCGCTGCAAGTATGATGG-3';
LOXL4 reverse, 5'-CCTGAGTCGCTGTTCCTGCT-3';
18S rRNA forward, 5'-GGCGACGACCCATTCG-3';
18S rRNA reverse, 5'-ACCCGTGGTCACCATGGTA-3'.

All samples were analyzed in triplicate as a minimum. After the reactions, the specificity of amplifications in each sample was confirmed by dissociation analysis, showing that each sample gave a single melting peak. The relative mRNA levels were normalized to the level of *18S rRNA*.

Western-blot analysis
Western blot analyses were performed as described elsewhere (31). In some immunoblotting analyses, samples were transferred onto an Immobilon-FL polyvinylidene fluoride (PVDF) membrane (Millipore Corp.) and probed with primary and IRDye 800CW- or IRDye 680-conjugated secondary antibodies (LI-COR Biosci.). Immunoreactive bands were detected using the Odyssey Infrared Imaging System (LI-COR Biosci.).

TGF-β bioassay
A mink lung cell line (TMLC) stably transfected with a plasminogen activator inhibitor-1 (PAI-1) promoter fused to luciferase was used for the analysis (38). Active TGF-β levels were measured as described elsewhere (32).

Hydroxyproline assay
Hydroxyproline content was measured as described elsewhere (26).

Hepatic biochemical markers
Serum alanine aminotransferase (ALT) level was determined using a standard kit (Genzyme Diagnostics P.E.I. Inc., Canada). Serum total protein (by the Biuret method), albumin (by the BCG method), total bilirubin (by the Azobilirubin method), and cholinesterase (by the p-Hydroxybenzolcholine method) levels were measured using the Hitachi 7180 Auto Analyzer (Japan).

***In vitro* assay using mouse hepatic stellate cell lines**
Control and Fn-null mouse hepatic stellate cell lines were established from adult primary hepatic stellate cell cultures under p21-null genetic background as described previously (26) and used for the analysis presented in this study. Briefly, hepatic stellate cells were isolated from adult Fn(flox/flox)/p21(-/-) mouse liver as parental cells, and subsequently those lines were treated with *Cre*-transducing adenovirus to delete *Fn-floxed genes* (Fn-null hepatic stellate cells). Established cell lines showed similar morphology and typical activated hepatic stellate cell phenotypes (26). To examine the effects of TGF-β1 on LOX production, hepatic stellate cells were cultured for 8 h with Dulbecco's modified Eagle's medium (DMEM) containing 8 % Fn-depleted FBS. The medium was then replaced with DMEM without FBS containing 0.2 mM ascorbic acid and 2 pM TGF-β1. Cells were then incubated for 18 h and used for the analysis. To examine the inhibitory effect of collagen crosslinking, cells were treated with β-aminopropionitrile (BAPN, 200 μM: Fisher Scientific) containing DMEM, 8 % Fn-depleted FBS, 0.2 mM ascorbic acid and 2 pM TGF-β1, then incubated for 7 days and used for the analysis. We confirmed that the concentration of BAPN used did not affect stellate cell proliferation (data not shown). To examine the effect of Fn on formed collagen stiffness, cells were cultured for 7 days with DMEM containing 8 % Fn-depleted FBS, 0.2 mM ascorbic acid and 10 μg/ml plasma Fn, then used for the analysis. To examine the signaling axis in TGF-β1-mediated LOX production, Fn-null stellate cells were cultured for 24 h with DMEM containing 8 % Fn-depleted FBS. The medium was then replaced with DMEM containing 0.2 mM ascorbic acid without FBS and with indicated supplements. Cells were preincubated for 1 hr, then treated with 2 pM TGF-β1, further incubated for 18 h, then analyzed. Where indicated, cultures contained 10 μM SIS3 (IC_{50}=3 μM) to inhibit Smad3, 10 μM LY294002 (IC_{50}=1.4 μM) to inhibit phosphatidylinositol 3 (PI3)-kinase, 10 μM PD169316 (IC_{50}=89 nM) to inhibit p38 MAP kinase, 5 μM 420119 (IC_{50}=40 nM) to inhibit c-Jun N-terminal kinase (JNK), and 20 μM PD98059 (IC_{50}=2 μM) to inhibit mitogen-activated protein kinase kinase (MEK)1/2. We confirmed that the concentration of the inhibitors used did not affect stellate cell proliferation (data not shown).

Data presentation and statistical analysis
All experiments were performed in triplicate as a minimum, on separate occasions, and the data shown were chosen as representative of results consistently observed. Results are presented as means ± standard deviation (S.D.). Differences between selected groups were analyzed using the Mann-Whitney *U* test. In cases where more than two groups were compared, the Steel-Dwass test was used. A *P* value of <0.05 was considered significant.

Results

More extensive fibrosis/cirrhosis in mice lacking Fn during CCl_4-induced advanced stages of chronic liver injury.
Based on our previous finding that Fn-deficiency did not interfere with reconstruction and resolution of collagen organization in initial stages of liver damage (26), we hypothesized that Fn-deficiency

may not affect the reconstruction of ECM architectures even in advanced stages of chronic liver damage. To address functional roles of Fn during this process, chronic liver fibrosis was induced in a well-established mouse model where injury is brought on by treatment with a liver-damaging agent, carbon tetrachloride (CCl_4, 0.5 ml/kg weight, twice a week for 17 weeks) (27). While increased expression of Fn protein was observed in control livers after injury, its expression in mutant livers (Fn(fl/fl)/*Mx-Cre+*) was remarkably low throughout the experimental period (time 0 through 17 weeks during CCl_4 injections). The Fn level in mutant livers at 17 weeks of CCl_4 treatment was only ~2% of that in control livers ($P < 0.01$) as shown by Western analysis (Fig. 1A; and data not shown). These data confirmed that neither Fn isoform was induced in mutant livers during advanced chronic injury. Anatomical and histological analyses revealed no abnormalities in Fn-null livers under standard laboratory conditions ((26), data not shown).

To determine whether Fn-deficiency affects CCl_4-induced liver damage during chronic injury, body weight changes, serum alanine aminotransferase (ALT, as a measure for hepatocyte damage) and albumin/globulin ratio (as a measure of net hepatic damage) were examined. These parameters showed similar patterns in both control and Fn-null livers during 17 weeks of CCl_4 treatment. Both showed no increase in body weight and a gradual decrease of ALT activity from 4 to 17 weeks and albumin/globulin ratio from 0 to 17 weeks (Fig. 1B, C), confirming the advanced stages of chronic liver injury in both control and mutant livers (39). Fibrosis was then assessed by Sirius Red staining, which allows visualization of collagen fibers. Histologically, both control and mutant livers developed complete fibrosis patterns throughout the regions such as the P-C bridge (between the portal area and the central vein) and C-C bridge formations (between the central veins) (Fig. 1D), indicating micronodular cirrhosis (27). Unexpectedly, Fn-null livers developed more extended and significant fibrosis. Approximately 12% of the livers were Sirius Red positive, representing a 3.2-fold increase over control livers (Fig. 1D, $P < 0.01$). Taken together, these findings indicate that prolonged and persistent chronic damage caused by 17 weeks of CCl_4 treatment does establish advanced liver fibrosis/micronodular cirrhosis in both control and Fn-null livers.

Elevated myofibroblast activity in mutant livers.

Myofibroblasts such as activated hepatic stellate cells play a central role in ECM remodeling upon liver injury. Immunofluorescence and Western analysis showed significantly more pronounced expression of α-smooth muscle actin (αSMA), a marker for myofibroblasts in Fn-null livers compared to controls at 17 weeks of CCl_4 treatment ($P < 0.05$; Fig. 2A, B). There was no obvious apoptosis or cell death in either liver type as shown by cleaved caspase 3 immunostaining and no picnotic nuclei with Hoechst 33342 staining at 17 weeks of CCl_4 treatment (Fig. 2C and data not shown).

Significant hepatic dysfunction and increased liver-tissue stiffness in mutant livers.

Next, we examined whether a lack of Fn affects hepatic functions during chronic injury (Fig. 3A-C). Subsequent analyses of serum hepatic biochemical markers (total bilirubin as a measure of hepatic excretory function; cholinesterase and albumin as a measure of hepatic protein synthesis) revealed no apparent differences between control and mutant livers until 8 weeks of CCl_4 treatment. In contrast, in the advanced stage at 17 weeks, mutant mice suffered from a significantly higher level of plasma total bilirubin (0.12 ± 0.02 mg/dl in control [$n = 6$] *vs.* 0.19 ± 0.04 mg/dl in mutant [$n = 6$], $P = 0.0074$) and lower level of cholinesterase (26.8 ± 1.5 IU/L in control [$n = 6$] *vs.* 23.4 ± 1.3 IU/L in mutant [$n = 6$], $P = 0.025$). Serum albumin levels were also decreased (3.37 ± 0.10 g/dl in control [$n = 6$] *vs.* 3.26 ± 0.15 g/dl in mutant [$n = 6$]) but without significance ($P = 0.39$). In addition, liver tissue stiffness as determined by AFM was significantly elevated in Fn-null livers compared to controls at 17 weeks of CCl_4 treatment (5,128 ± 553.6 MPa in mutant vs. 3,313 ± 835.2 MPa in control ($n = 9$); $P < 0.05$, Fig. 3D-3G).

Elevated production of latent TGF-β complexes and increased local TGF-β bioavailability in mutant livers.

Fn is associated with latent TGF-β complexes when incorporated into the ECM (16,40) and local TGF-β activity is elevated in Fn-null livers in initial stages following liver injury (26,41). Hence, the effect of Fn-deficiency on the production of latent complexes of TGF-β and local TGF-β bioavailability during advanced chronic liver injury was also investiaged. Pronounced depositions of LAP and of LTBP-1, -3 and -4 in the ECM of mutant livers were shown by immunohistochemistry at 17 weeks of CCl_4 treatment. Interestingly, fibrillar structures were

present even in the absence of Fn (Fig. 4A). Furthermore, the TGF-β activity in mutant livers was significantly higher than in controls at both 8 and 17 weeks of CCl_4 treatment (Fig. 4B, $P < 0.05$), indicating constitutively higher levels of active TGF-β in Fn-null livers during chronic liver injury.

TGF-β promotes the initiation of myofibroblast phenotypes and TGF-β1 alone sufficiently initiates stellate cell activation and transdifferentiation into myofibroblasts after liver injury, whereas Fn extra domain-A (EDA) promotes stellate cell motility but not transdifferentiation into myofibroblasts *in vitro* (26,42). Latent TGF-β that is activated in response to injury binds to the TGF-β type I receptor, which then phosphorylates the C-terminal regions of Smad 2/3 transcription factors. Activated Smads translocate to the nucleus where they are involved in the regulation of gene expression (43,44). Indeed, Fn-null livers showed a significantly increased number of nuclear phospho (p)-Smad2/3-positive nonparenchymal cells ($P < 0.01$) (Fig. 4C). Since constitutively elevated local TGF-β activity was demonstrated in Fn-null livers during chronic liver damage ($P < 0.05$, Fig. 4B), the functional link between TGF-β and myofibroblastic phenotypes at 17 weeks of CCl_4 treatment was further addressed by double immunohistochemical staining. Fn-null livers showed a significantly increased number of p-Smad2/3 and αSMA double-positive myofibroblasts (31.3 ± 5.5 cells/field in mutant; field = 0.37 mm^2 [$n = 10$] *vs.* 9.8 ± 3.3 cells/field in control [$n = 10$], $P < 0.01$) (Fig. 4D). No nuclear localization of p-Smad2/3 was noted in either non-injured control or Fn-null livers (data now shown).

More disorganized collagen networks with increased lysyl oxidase expressions in mutant livers.

Based on these data, we hypothesized that the collagenous ECM fibrillar network formed in the absence of Fn may differ functionally from Fn-mediated collagenous fibrils, and the more extended fibrosis found in mutant livers (Fig. 1D) was associated with the impaired hepatic functions. Collagen network formation occurs as a multi-step process and contributes to ECM remodeling and maintenance upon tissue damage (45). Therefore, the expression, assembly and degradation levels of the major collagens, type I and III, in the advanced stages of chronic damage was next examined. Highly-disorganized collagen matrices were induced in Fn-null livers. Immunofluorescent observation revealed that extensive networks of type I and III collagen were diffusely distributed in the ECM (Fig. 5A). Type I collagen mRNA levels was also significantly increased in Fn-null livers ($P < 0.05$, Fig. 5B). Collagen networks displayed more disorganized arrangements and significantly larger angular deviation in mutant livers as assessed by Sirius Red stained-samples under the polarized microscope (Fig. 5C-5E). In contrast, control livers formed well-organized, linear type III and type I collagen networks (Fig. 5A, 5C-5E). There were no significant differences in the expression of collagen-related matrix metalloproteinase (MMP) *MMP8* and *MMP13* mRNA levels (Fig. 5F), suggesting that collagen degrading enzymes did not play major roles.

Since type V collagen is an essential element for type III/I collagen fibrillogenesis *in vitro* when Fn is absent (26), the contribution of type V collagen to advanced stages of chronic liver remodeling at 17 weeks of CCl_4 treatment was then determined. Significantly increased deposition and assembly of type V collagen was detected in Fn-null livers in comparison with controls and the localization of assembled fibrils often overlapped with type I collagen fibrils (Fig. 6A). Increased expression of type V collagen mRNA (~1.5-fold) was also observed in mutant livers compared to controls, although the difference was not statistically significant (Fig. 6B). Subsequent ultrastructural analysis using TEM revealed that the mean diameter of collagen fibrils was identical (47.0 ± 9.7 nm in mutant *vs.* 48.3 ± 8.9 nm in control [$n = 1{,}500$ fibrils in each]) (Fig. 6C, D). It is known that the diameter of formed type I collagen fibrils is inversely proportional to the type V/type I collagen ratio (46-48). Indeed, a ~33% increase in the number of thinner (30-40 nm diameter) and a ~21% decrease in the number of thicker (50-60 nm diameter) collagen fibril-subpopulations was found in Fn-null livers compared to controls (Fig. 6D, right panel). Such thinner collagen fibril-subpopulations were also confirmed by AFM analysis (Fig. 3G). Importantly, a significantly increased number of collagen fibrils was demonstrated in mutant livers compared to controls (48.6 ± 7.0 fibrils/ 0.25 μm^2 in mutant vs. 41.7 ± 4.6 fibrils/ 0.25 μm^2 in control ($n = 18$); $P < 0.01$, Fig. 6E). The increased fibril number correlated with an increase in hepatic net collagen amount measured by hydroxyproline content ($P < 0.05$, Fig. 6F). Thus, these results indicate that elimination of Fn results in thinner and increased number of collagen fibril organizations/assemblies and suggest both quantitative and qualitative differences between Fn- and type V collagen-mediated type I collagen fibril network formation following tissue injury.

Collagen crosslinking by LOX family members accompanies tissue fibrosis and stiffens tissues (12). Elevated expression of LOX and its subfamily, LOX-like protein (LOXL)2 is detected in both human fibrotic diseases and rodent injury models, and myofibroblasts such as activated hepatic stellate cells are the likely major cellular source of LOX in liver injury (49,50). Since significantly increased liver tissue stiffness alongside the deterioration of net hepatic function was demonstrated in Fn-null livers at 17 weeks of CCl_4 treatment, the functional link between the lack of Fn and LOX expression levels was addressed. LOX and LOXL1-4 mRNA levels were all upregulated in Fn-null livers compared to controls, and LOX was found to be most upregulated in mutant livers (~2.64-fold) compared to controls ($P < 0.01$, Fig. 7A). Therefore, we determined whether elevated TGF-β bioavailability due to absence of Fn is directly involved in the production of LOX in activated hepatic stellate cells *in vitro*. The treatment of Fn-null hepatic stellate cell lines with 2 pM TGF-β1 led to the release of a significant amount of active LOX proteins compared to parental cells (2.46 ± 0.13-fold upregulation in Fn-null vs. 1.60 ± 0.15-fold upregulation in control in response to TGF-β1, $P < 0.01$), whereas no obvious differences in LOX protein levels were observed between them under untreated conditions (Fig. 7B). We further investigated the signaling axis for TGF-β1-mediated LOX expression in Fn-null hepatic stellate cells. Immunocytochemical analysis revealed a significant elevation of LOX expression in Fn-null hepatic stellate cells in response to TGF-β1 (Fig. 7C). Application of Smad3 inhibitor SIS3 following TGF-β1 treatment significantly inhibited (~42.0%) LOX expression in Fn-null hepatic stellate cells. In addition, PI3-kinase inhibitor LY294002 significantly inhibited LOX expression (~38.1%), although to a lesser degree (Fig. 7C). This demonstrates the involvement of both canonical and non-canonical Smad such as PI3 kinase-mediated pathways in TGF-β1-mediated LOX expression in hepatic stellate cells.

Fn-null hepatic stellate cells do not organize type I collagen fibril network in culture, and TGF-β1 can induce type I collagen assembly (26). Therefore, the functional link between TGF-β1-induced LOX and structural and mechanical integrity of collagen fibril network in Fn-null hepatic stellate cells was addressed. Indeed, TGF-β1-induced collagen fibril stiffness in Fn-null hepatic stellate cells was significantly higher compared to control (parental) cells (Fig. 8A, $P < 0.01$). Treatment of Fn-null stellate cells with 2 pM TGF-β1 and LOX inhibitor β-aminopropionitrile (BAPN, 200 μM) resulted in the disruption of TGF-β-induced fine collagen fibril networks and significantly reduced collagen fibril stiffness ($P < 0.01$) (Fig. 8A, B). Importantly, treatment of Fn-null stellate cells with 10 μg/ml plasma Fn recovered collagen fibril stiffness to control (parental) cell levels (Fig. 8C). Thus, taken together, these findings indicate that elevated TGF-β bioavailability in Fn-null livers induces more active myofibroblasts and sustains their activated phenotypes. As a consequence of this, these myofibroblasts develop more accumulated, disorganized, and LOX-mediated tightly cross-linked collagenous ECMs during advanced chronic liver damage, which thereby results in the significant deterioration of net hepatic function.

Discussion

Our current comprehensive genetic studies with a Fn-deficient animal model provide the following compelling evidence. (1) Elimination of Fn results in elevated local TGF-β activity and continuously increased intracellular TGF-β signaling in activated hepatic stellate cells (myofibroblasts). This results in the development of more advanced liver fibrosis/cirrhosis in Fn-null livers. (2) Fn-null livers exhibit significantly increased LOX expression in chronic liver injury, and Fn-null hepatic stellate cells are a target for the release of active LOX in response to TGF-β1 through both canonical and non-canonical Smad pathways. Thus, we propose that there are the functional links between Fn-mediated control of TGF-β bioavailability and collagen fibril stiffness regulated by LOX. We suggest that such regulatory mechanisms by Fn could be translated for a potential therapeutic target in other chronic fibrotic diseases.

Our current findings in Fn-null mouse livers are consistent with the fact that elevated TGF-β activity induces enhanced differentiation and activation of quiescent fibroblastic cells with a myofibroblastic phenotype (induction of αSMA) in response to tissue damage (5,7). The expression level of αSMA is directly related to the contractile activity of myofibroblasts, which cause tissue contractures (51). This suggests that persistently elevated TGF-β activity due to the lack of Fn induces more highly contractile myofibroblasts and leads to greater ECM secretion accompanied with increased LOX-mediated collagen crosslinking. However, collagen

network reorganization in adult tissues in response to injury is mediated by both Fn and TGF-β-induced type V collagen (26), and our results show both quantitative and qualitative differences between Fn- and type V collagen-mediated type I collagen fibril network formation. Therefore, while the contribution of type V collagen-nucleated collagen fibrogenesis in adult tissues is largely undetermined, our findings support the hypothesis that the accumulation of type V collagen-mediated ECMs during persistent chronic damage has an influence on disorganized ECM 3-dimensional architecture. Such phenotypes occurring beyond the early stages following tissue damage could contribute to the critical turning point from normal to abnormal healing *in vivo*. Consequently, more disorganized and rigid ECMs remarkably impede organ architecture and function. Indeed, accumulating evidence indicates that locally activated TGF-β plays a significant role in the development of liver fibrosis (52-54).

Earlier studies have shown that collagen cross-linking mediated by LOX leads to cancer progression by enhancing ECM receptor integrin signaling (11) and that inhibition of LOX activity partially prevents tissue stiffness following injury (55). Consistent with previous *in vitro* and *in vivo* observations, (11,56,57), our findings indicate that inhibition of collagen cross linking by BAPN affects TGF-β-induced structural and mechanical integrity of collagenous ECM networks in Fn-null hepatic stellate cells. We have demonstrated functional links between tissue/organ functions and regulatory mechanisms of LOX underlying chronic fibrotic disease such as liver fibrosis/cirrhosis. Bone morphogenic protein 1 (BMP 1), an extracellular metalloproteinase, and periostin, a secretory protein in connective tissues, are major activators of LOX and interact with Fn (58,59). Fn-null embryonic fibroblasts dramatically decrease proteolytic processing of the 45 kDa LOX proenzyme to the 32 kDa active form without changing BMP1 levels compared to control cells, suggesting the regulatory role of Fn matrix in LOX catalytic activity (60). In contrast, we have shown that Fn-null hepatic stellate cells release significant amount of active LOX in response to TGF-β1 without Fn matrix. Interestingly, this TGF-β1-LOX signaling axis in Fn-null hepatic stellate cells is mediated through both canonical and non-canonical pathways (61). A very recent observation has documented that the expression level of periostin is significantly upregulated in both acute and chronic liver injury, and TGF-β1 can induce periostin in hepatic stellate cells *in vitro* (62). Thus, periostin is likely to be involved in TGF-β1-induced LOX activation in Fn-null hepatic stellate cells as cell type specific phenotyptes.

Little insight into the pathophysiological roles of Fn has emerged from studies of genetic changes in humans. There are no documented cases of Fn-null patients, the nearest condition being familial glomerulonephritis in which there are mutations in the type III modules of Fn (63). Whilst complete Fn-null mice show an embryonic lethal phenotype (64), experimental evidence has documented that skin wounds heal normally in mice lacking plasma type Fn (30), hence an absolute requirement for Fn in response to adult tissue damage has been speculative. The current findings imply that Fn regulates the balance between active and inactive (latent) TGF-β, which in turn modulates ECM production and remodeling following injury, and consequently retains adult tissue/organ functions. A number of genetic studies suggest that the absence of, or a mutation in, LLC-binding ECMs such as fibrillin-1 and -2 results in increased TGF-β activity and Smad signaling, whereas the absence of, or mutation in, LTBPs results in decreased activity and signaling (65-70). We have demonstrated that the absence of Fn results in increased TGF-β bioavailability following organ injury. A possible explanation for elevated TGF-β bioavailability is that the deficiency of LLC-binding ECMs, as seen in this Fn-null model, decreases the matrix sequestration of LLCs, which thereby renders latent TGF-β more accessible for activation with negative consequences for cellular functions (71). In contrast, there were very limited *in vivo* observations for negative regulation of TGF-β bioavailability by Fn. A recent study reveals that the inhibition of cell-mediated Fn matrix assembly without affecting its production by peptide pUR4 shows the normal release of active TGF-β in hepatic stellate cells *in vitro* (72). However, Fn matrix networks play crucial roles in many important biological events and in adult homeostasis (21,22). Fn matrix networks promote parenchymal cell survival such as hepatocytes following liver damage (23), and the elimination of Fn extradomain-A (EDA) splicing domain results in a shorter life span (73). Therefore, the regulation of TGF-β bioavailability by Fn with retaining Fn matrix networks would be essential elements for long-term anti-fibrotic strategies in chronic fibrotic diseases to preserve tissue/organ function and homeostasis.

Acknowledgments
We thank Zhuo Chang (School of Engineering, University of Liverpool) for expert technical assistance with the atomic force microscopy studies, and Dr. Masahide Yoshikawa for assistance of serological analysis. We also thank Dr. Harihara Baskaran for valuable comments and suggestions, and Dr. Emma Stephenson for editorial assistance.

Grant Support
This work was supported by National Institutes of Health research grant DK074538 (to T. Sakai). We are also grateful to the Institute of Translational Medicine, University of Liverpool for support (to T. Sakai.).

Conflict of interest
The authors disclose no conflicts.

Author contributions
Takao Sakai conceived ideas, designed experiments, and supervised the project. Ayumi Iwasaki, Keiko Sakai, Kei Moriya, Takayoshi Miyazono, and Satoshi Yasumura performed experiments. Douglas Keene carried out transmission electron microscopy studies, and Riaz Akhtar carried out atomic force microscopy studies. Takako Sasaki generated anti-type I, III and V collagen, LAP, LTBP-3 and 4, and LOX antibodies. Ayumi Iwasaki, Keiko Sakai, Kei Moriya, Riaz Akhtar, Takayoshi Miyazono, Satoshi Yasumura, Masatoshi Watanabe, Shin Morishita, and Takao Sakai analyzed the data. Takao Sakai wrote and edited the manuscript.

References

1. Diehl, A. M., and Chute, J. (2013) Underlying potential: cellular and molecular determinants of adult liver repair. *The Journal of clinical investigation* **123**, 1858-1860
2. Bataller, R., and Brenner, D. A. (2005) Liver fibrosis. *The Journal of clinical investigation* **115**, 209-218
3. Friedman, S. L. (2010) Evolving challenges in hepatic fibrosis. *Nat Rev Gastroenterol Hepatol* **7**, 425-436
4. Schuppan, D., and Kim, Y. O. (2013) Evolving therapies for liver fibrosis. *The Journal of clinical investigation* **123**, 1887-1901
5. Wallace, K., Burt, A. D., and Wright, M. C. (2008) Liver fibrosis. *Biochem J* **411**, 1-18
6. Forbes, S. J., and Parola, M. (2011) Liver fibrogenic cells. *Best practice & research. Clinical gastroenterology* **25**, 207-217
7. Hinz, B., Phan, S. H., Thannickal, V. J., Galli, A., Bochaton-Piallat, M. L., and Gabbiani, G. (2007) The myofibroblast: one function, multiple origins. *The American journal of pathology* **170**, 1807-1816
8. Kolacna, L., Bakesova, J., Varga, F., Kostakova, E., Planka, L., Necas, A., Lukas, D., Amler, E., and Pelouch, V. (2007) Biochemical and biophysical aspects of collagen nanostructure in the extracellular matrix. *Physiological research / Academia Scientiarum Bohemoslovaca* **56 Suppl 1**, S51-60
9. Lucero, H. A., and Kagan, H. M. (2006) Lysyl oxidase: an oxidative enzyme and effector of cell function. *Cell Mol Life Sci* **63**, 2304-2316
10. Csiszar, K. (2001) Lysyl oxidases: a novel multifunctional amine oxidase family. *Prog Nucleic Acid Res Mol Biol* **70**, 1-32
11. Levental, K. R., Yu, H., Kass, L., Lakins, J. N., Egeblad, M., Erler, J. T., Fong, S. F., Csiszar, K., Giaccia, A., Weninger, W., Yamauchi, M., Gasser, D. L., and Weaver, V. M. (2009) Matrix crosslinking forces tumor progression by enhancing integrin signaling. *Cell* **139**, 891-906
12. van der Slot, A. J., van Dura, E. A., de Wit, E. C., De Groot, J., Huizinga, T. W., Bank, R. A., and Zuurmond, A. M. (2005) Elevated formation of pyridinoline cross-links by profibrotic cytokines is associated with enhanced lysyl hydroxylase 2b levels. *Biochim Biophys Acta* **1741**, 95-102
13. Gressner, A. M., Weiskirchen, R., Breitkopf, K., and Dooley, S. (2002) Roles of TGF-beta in hepatic fibrosis. *Front Biosci* **7**, d793-807
14. Hayashi, H., and Sakai, T. (2012) Biological Significance of Local TGF-beta Activation in Liver Diseases. *Frontiers in physiology* **3**, 12
15. Dallas, S. L., Sivakumar, P., Jones, C. J., Chen, Q., Peters, D. M., Mosher, D. F., Humphries, M. J., and Kielty, C. M. (2005) Fibronectin regulates latent transforming growth factor-beta (TGF beta) by controlling matrix assembly of latent TGF beta-binding protein-1. *The Journal of biological chemistry* **280**, 18871-18880
16. Rifkin, D. B. (2005) Latent transforming growth factor-beta (TGF-beta) binding proteins: orchestrators of TGF-beta availability. *The Journal of biological chemistry* **280**, 7409-7412
17. Margadant, C., and Sonnenberg, A. (2010) Integrin-TGF-beta crosstalk in fibrosis, cancer and wound healing. *EMBO Rep* **11**, 97-105
18. Sheppard, D. (2006) Transforming growth factor beta: a central modulator of pulmonary and airway inflammation and fibrosis. *Proc Am Thorac Soc* **3**, 413-417
19. Varga, J., and Pasche, B. (2009) Transforming growth factor beta as a therapeutic target in systemic sclerosis. *Nat Rev Rheumatol* **5**, 200-206
20. Nishimura, S. L. (2009) Integrin-mediated transforming growth factor-beta activation, a potential therapeutic target in fibrogenic disorders. *The American journal of pathology* **175**, 1362-1370
21. Hynes, R. O. (1990) *Fibronectins*, Springer-Verlag, New York
22. Mosher, D. F. (1989) *Fibronectin*, Academic Press, San Diego
23. Moriya, K., Sakai, K., Yan, M. H., and Sakai, T. (2012) Fibronectin is essential for survival but is dispensable for proliferation of hepatocytes in acute liver injury in mice. *Hepatology (Baltimore, Md.)* **56**, 311-321
24. Velling, T., Risteli, J., Wennerberg, K., Mosher, D. F., and Johansson, S. (2002) Polymerization of type I and III collagens is dependent on fibronectin and enhanced by integrins alpha 11beta 1 and alpha 2beta 1. *The Journal of biological chemistry* **277**, 37377-37381

25. Sottile, J., Shi, F., Rublyevska, I., Chiang, H. Y., Lust, J., and Chandler, J. (2007) Fibronectin-dependent collagen I deposition modulates the cell response to fibronectin. *Am J Physiol Cell Physiol* **293**, C1934-1946
26. Moriya, K., Bae, E., Honda, K., Sakai, K., Sakaguchi, T., Tsujimoto, I., Kamisoyama, H., Keene, D. R., Sasaki, T., and Sakai, T. (2011) A fibronectin-independent mechanism of collagen fibrillogenesis in adult liver remodeling. *Gastroenterology* **140**, 1653-1663
27. Constandinou, C., Henderson, N., and Iredale, J. P. (2005) Modeling liver fibrosis in rodents. *Methods Mol Med* **117**, 237-250
28. Nowack, H., Gay, S., Wick, G., Becker, U., and Timpl, R. (1976) Preparation and use in immunohistology of antibodies specific for type I and type III collagen and procollagen. *J Immunol Methods* **12**, 117-124
29. Timpl, R. (1982) Antibodies to collagens and procollagens. *Methods in enzymology* **82 Pt A**, 472-498
30. Sakai, T., Johnson, K. J., Murozono, M., Sakai, K., Magnuson, M. A., Wieloch, T., Cronberg, T., Isshiki, A., Erickson, H. P., and Fassler, R. (2001) Plasma fibronectin supports neuronal survival and reduces brain injury following transient focal cerebral ischemia but is not essential for skin-wound healing and hemostasis. *Nat Med* **7**, 324-330
31. Sakai, T., Li, S., Docheva, D., Grashoff, C., Sakai, K., Kostka, G., Braun, A., Pfeifer, A., Yurchenco, P. D., and Fassler, R. (2003) Integrin-linked kinase (ILK) is required for polarizing the epiblast, cell adhesion, and controlling actin accumulation. *Genes Dev* **17**, 926-940
32. Maeda, T., Sakabe, T., Sunaga, A., Sakai, K., Rivera, A. L., Keene, D. R., Sasaki, T., Stavnezer, E., Iannotti, J., Schweitzer, R., Ilic, D., Baskaran, H., and Sakai, T. (2011) Conversion of mechanical force into TGF-beta-mediated biochemical signals. *Curr Biol* **21**, 933-941
33. Whittaker, P., and Przyklenk, K. (2009) Fibrin architecture in clots: a quantitative polarized light microscopy analysis. *Blood Cells Mol Dis* **42**, 51-56
34. Katoh, K., Hammar, K., Smith, P. J., and Oldenbourg, R. (1999) Arrangement of radial actin bundles in the growth cone of Aplysia bag cell neurons shows the immediate past history of filopodial behavior. *Proc Natl Acad Sci U S A* **96**, 7928-7931
35. Madibally, S. V., Solomon, V., Mitchell, R. N., Van De Water, L., Yarmush, M. L., and Toner, M. (2003) Influence of insulin therapy on burn wound healing in rats. *J Surg Res* **109**, 92-100
36. Papi, M., Paoletti, P., Geraghty, B., and Akhtar, R. (2014) Nanoscale characterization of the biomechanical properties of collagen fibrils in the sclera. *Applied Physics Letters* **104**, 103703
37. Honda, K., Sakaguchi, T., Sakai, K., Schmedt, C., Ramirez, A., Jorcano, J. L., Tarakhovsky, A., Kamisoyama, H., and Sakai, T. (2007) Epidermal hyperplasia and papillomatosis in mice with a keratinocyte-restricted deletion of csk. *Carcinogenesis* **28**, 2074-2081
38. Abe, M., Harpel, J. G., Metz, C. N., Nunes, I., Loskutoff, D. J., and Rifkin, D. B. (1994) An assay for transforming growth factor-beta using cells transfected with a plasminogen activator inhibitor-1 promoter-luciferase construct. *Anal Biochem* **216**, 276-284
39. Schuppan, D., and Afdhal, N. H. (2008) Liver cirrhosis. *Lancet* **371**, 838-851
40. Hynes, R. O. (2009) The extracellular matrix: not just pretty fibrils. *Science* **326**, 1216-1219
41. Kawelke, N., Vasel, M., Sens, C., Au, A., Dooley, S., and Nakchbandi, I. A. (2011) Fibronectin protects from excessive liver fibrosis by modulating the availability of and responsiveness of stellate cells to active TGF-beta. *PLoS One* **6**, e28181
42. Olsen, A. L., Sackey, B. K., Marcinkiewicz, C., Boettiger, D., and Wells, R. G. (2012) Fibronectin extra domain-A promotes hepatic stellate cell motility but not differentiation into myofibroblasts. *Gastroenterology* **142**, 928-937 e923
43. Massague, J., Seoane, J., and Wotton, D. (2005) Smad transcription factors. *Genes Dev* **19**, 2783-2810
44. Moustakas, A., and Heldin, C. H. (2009) The regulation of TGFbeta signal transduction. *Development* **136**, 3699-3714
45. Canty, E. G., and Kadler, K. E. (2005) Procollagen trafficking, processing and fibrillogenesis. *Journal of cell science* **118**, 1341-1353
46. Adachi, E., and Hayashi, T. (1986) In vitro formation of hybrid fibrils of type V collagen and type I collagen. Limited growth of type I collagen into thick fibrils by type V collagen. *Connect Tissue Res* **14**, 257-266

47. Wenstrup, R. J., Florer, J. B., Brunskill, E. W., Bell, S. M., Chervoneva, I., and Birk, D. E. (2004) Type V collagen controls the initiation of collagen fibril assembly. *The Journal of biological chemistry* **279**, 53331-53337
48. Birk, D. E. (2001) Type V collagen: heterotypic type I/V collagen interactions in the regulation of fibril assembly. *Micron* **32**, 223-237
49. Perepelyuk, M., Terajima, M., Wang, A. Y., Georges, P. C., Janmey, P. A., Yamauchi, M., and Wells, R. G. (2013) Hepatic stellate cells and portal fibroblasts are the major cellular sources of collagens and lysyl oxidases in normal liver and early after injury. *Am J Physiol Gastrointest Liver Physiol* **304**, G605-614
50. Barry-Hamilton, V., Spangler, R., Marshall, D., McCauley, S., Rodriguez, H. M., Oyasu, M., Mikels, A., Vaysberg, M., Ghermazien, H., Wai, C., Garcia, C. A., Velayo, A. C., Jorgensen, B., Biermann, D., Tsai, D., Green, J., Zaffryar-Eilot, S., Holzer, A., Ogg, S., Thai, D., Neufeld, G., Van Vlasselaer, P., and Smith, V. (2010) Allosteric inhibition of lysyl oxidase-like-2 impedes the development of a pathologic microenvironment. *Nat Med* **16**, 1009-1017
51. Guyot, C., Lepreux, S., Combe, C., Doudnikoff, E., Bioulac-Sage, P., Balabaud, C., and Desmouliere, A. (2006) Hepatic fibrosis and cirrhosis: the (myo)fibroblastic cell subpopulations involved. *Int J Biochem Cell Biol* **38**, 135-151
52. Kondou, H., Mushiake, S., Etani, Y., Miyoshi, Y., Michigami, T., and Ozono, K. (2003) A blocking peptide for transforming growth factor-beta1 activation prevents hepatic fibrosis in vivo. *Journal of hepatology* **39**, 742-748
53. Drews, F., Knobel, S., Moser, M., Muhlack, K. G., Mohren, S., Stoll, C., Bosio, A., Gressner, A. M., and Weiskirchen, R. (2008) Disruption of the latent transforming growth factor-beta binding protein-1 gene causes alteration in facial structure and influences TGF-beta bioavailability. *Biochim Biophys Acta* **1783**, 34-48
54. Wang, B., Dolinski, B. M., Kikuchi, N., Leone, D. R., Peters, M. G., Weinreb, P. H., Violette, S. M., and Bissell, D. M. (2007) Role of alphavbeta6 integrin in acute biliary fibrosis. *Hepatology (Baltimore, Md.)* **46**, 1404-1412
55. Georges, P. C., Hui, J. J., Gombos, Z., McCormick, M. E., Wang, A. Y., Uemura, M., Mick, R., Janmey, P. A., Furth, E. E., and Wells, R. G. (2007) Increased stiffness of the rat liver precedes matrix deposition: implications for fibrosis. *Am J Physiol Gastrointest Liver Physiol* **293**, G1147-1154
56. Zhao, R., Chen, C. S., and Reich, D. H. (2014) Force-driven evolution of mesoscale structure in engineered 3D microtissues and the modulation of tissue stiffening. *Biomaterials* **35**, 5056-5064
57. Mammoto, A., Mammoto, T., Kanapathipillai, M., Wing Yung, C., Jiang, E., Jiang, A., Lofgren, K., Gee, E. P., and Ingber, D. E. (2013) Control of lung vascular permeability and endotoxin-induced pulmonary oedema by changes in extracellular matrix mechanics. *Nature communications* **4**, 1759
58. Huang, G., Zhang, Y., Kim, B., Ge, G., Annis, D. S., Mosher, D. F., and Greenspan, D. S. (2009) Fibronectin binds and enhances the activity of bone morphogenetic protein 1. *The Journal of biological chemistry* **284**, 25879-25888
59. Maruhashi, T., Kii, I., Saito, M., and Kudo, A. (2010) Interaction between periostin and BMP-1 promotes proteolytic activation of lysyl oxidase. *The Journal of biological chemistry* **285**, 13294-13303
60. Fogelgren, B., Polgar, N., Szauter, K. M., Ujfaludi, Z., Laczko, R., Fong, K. S., and Csiszar, K. (2005) Cellular fibronectin binds to lysyl oxidase with high affinity and is critical for its proteolytic activation. *The Journal of biological chemistry* **280**, 24690-24697
61. Voloshenyuk, T. G., Landesman, E. S., Khoutorova, E., Hart, A. D., and Gardner, J. D. (2011) Induction of cardiac fibroblast lysyl oxidase by TGF-beta1 requires PI3K/Akt, Smad3, and MAPK signaling. *Cytokine* **55**, 90-97
62. Huang, Y., Liu, W., Xiao, H., Maitikabili, A., Lin, Q., Wu, T., Huang, Z., Liu, F., Luo, Q., and Ouyang, G. (2015) Matricellular protein periostin contributes to hepatic inflammation and fibrosis. *The American journal of pathology* **185**, 786-797
63. Castelletti, F., Donadelli, R., Banterla, F., Hildebrandt, F., Zipfel, P. F., Bresin, E., Otto, E., Skerka, C., Renieri, A., Todeschini, M., Caprioli, J., Caruso, R. M., Artuso, R., Remuzzi, G., and Noris, M. (2008) Mutations in FN1 cause glomerulopathy with fibronectin deposits. *Proc Natl Acad Sci U S A* **105**, 2538-2543

64. George, E. L., Georges-Labouesse, E. N., Patel-King, R. S., Rayburn, H., and Hynes, R. O. (1993) Defects in mesoderm, neural tube and vascular development in mouse embryos lacking fibronectin. *Development* **119**, 1079-1091
65. Neptune, E. R., Frischmeyer, P. A., Arking, D. E., Myers, L., Bunton, T. E., Gayraud, B., Ramirez, F., Sakai, L. Y., and Dietz, H. C. (2003) Dysregulation of TGF-beta activation contributes to pathogenesis in Marfan syndrome. *Nature genetics* **33**, 407-411
66. Nistala, H., Lee-Arteaga, S., Smaldone, S., Siciliano, G., Carta, L., Ono, R. N., Sengle, G., Arteaga-Solis, E., Levasseur, R., Ducy, P., Sakai, L. Y., Karsenty, G., and Ramirez, F. (2010) Fibrillin-1 and -2 differentially modulate endogenous TGF-beta and BMP bioavailability during bone formation. *The Journal of cell biology* **190**, 1107-1121
67. Koli, K., Wempe, F., Sterner-Kock, A., Kantola, A., Komor, M., Hofmann, W. K., von Melchner, H., and Keski-Oja, J. (2004) Disruption of LTBP-4 function reduces TGF-beta activation and enhances BMP-4 signaling in the lung. *The Journal of cell biology* **167**, 123-133
68. Yoshinaga, K., Obata, H., Jurukovski, V., Mazzieri, R., Chen, Y., Zilberberg, L., Huso, D., Melamed, J., Prijatelj, P., Todorovic, V., Dabovic, B., and Rifkin, D. B. (2008) Perturbation of transforming growth factor (TGF)-beta1 association with latent TGF-beta binding protein yields inflammation and tumors. *Proc Natl Acad Sci U S A* **105**, 18758-18763
69. Loeys, B. L., Gerber, E. E., Riegert-Johnson, D., Iqbal, S., Whiteman, P., McConnell, V., Chillakuri, C. R., Macaya, D., Coucke, P. J., De Paepe, A., Judge, D. P., Wigley, F., Davis, E. C., Mardon, H. J., Handford, P., Keene, D. R., Sakai, L. Y., and Dietz, H. C. (2010) Mutations in fibrillin-1 cause congenital scleroderma: stiff skin syndrome. *Sci Transl Med* **2**, 23ra20
70. Mazzieri, R., Jurukovski, V., Obata, H., Sung, J., Platt, A., Annes, E., Karaman-Jurukovska, N., Gleizes, P. E., and Rifkin, D. B. (2005) Expression of truncated latent TGF-beta-binding protein modulates TGF-beta signaling. *Journal of cell science* **118**, 2177-2187
71. Ramirez, F., and Rifkin, D. B. (2009) Extracellular microfibrils: contextual platforms for TGFbeta and BMP signaling. *Curr Opin Cell Biol* **21**, 616-622
72. Altrock, E., Sens, C., Wuerfel, C., Vasel, M., Kawelke, N., Dooley, S., Sottile, J., and Nakchbandi, I. A. (2015) Inhibition of fibronectin deposition improves experimental liver fibrosis. *Journal of hepatology* **62**, 625-633
73. Muro, A. F., Chauhan, A. K., Gajovic, S., Iaconcig, A., Porro, F., Stanta, G., and Baralle, F. E. (2003) Regulated splicing of the fibronectin EDA exon is essential for proper skin wound healing and normal lifespan. *The Journal of cell biology* **162**, 149-160

Abbreviations

αSMA, α-smooth muscle actin; ALT, alanine aminotransferase; AFM, atomic force microscopy; BAPN, β-aminopropionitrile; BMP 1, Bone morphogenic protein 1; CCl_4, carbon tetrachloride; DAPI, 4'6-diamidino-2-phenylindole; ECM, extracellular matrix; FITC, fluorescein isothiocyanate; Fn, fibronectin; LAP, latency associated protein; LLC, large latent complex; LOX, lysyl oxidase; LTBP, latent TGF-β-binding protein; MMP, matrix metalloproteinase; mAb, monoclonal antibody; PCR, polymerase chain reaction; pAb, polyclonal antibody; pI-pC, polyinosinic-polycytidic acid; PVDF, polyvinylidene fluoride; TEM, transmission electron microscopy; TGF-β, transforming growth factor-β

Figure Legends

Fig. 1. Liver fibrosis/cirrhosis developing during CCl_4-induced (0.5 ml/kg weight) chronic liver injury is greater in mice lacking liver Fn (Control, wild-type with CCl_4; LivFn-null, mutant with CCl_4; Untreated, wild-type without CCl_4 treatment).
(**A**) Generation of advanced chronic liver fibrosis/cirrhosis by CCl_4 in mice lacking liver Fn (Fn(f/f)/*Mx-Cre+*). (Upper panels) Western blot analysis of Fn (plasma and cellular types) in liver tissue lysates from control and mutant mice before (0 week) and at 17 weeks of CCl_4 treatment. (Lower panel) Analysis of Fn intensities at 17 weeks of CCl_4 treatment. Fn expression levels are shown relative to the control value of 100 (percent of control). Error bars represent standard deviation (n = 5 for each group). Note that the depletion of Fn in mutant livers is ~98% (**, P < 0.01).
(**B**) Analysis of body weight. Data are means ± S.D. (*n* = 5 for each group). Note that both control and mutant body weights show similar patterns during the continuous phase of hepatic damage caused by CCl_4.
(**C**) Serum alanine aminotransferase (ALT) levels and albumin/globulin (A/G) ratio. Data are means ± S.D. (*n* = 6 for each group). Note that while both ALT levels and A/G ratio are gradually decreased in both control and mutant mice, they show similar patterns throughout the process.
(**D**) Upper panels: Mice lacking Fn develop more pronounced liver fibrosis/cirrhosis, as identified by Sirius Red staining at 17 weeks of CCl_4 treatment. Bar = 100 μm. Lower panel: Quantification of fibrosis at 17 weeks of CCl_4 treatment based on Sirius Red staining. Data are means ± S.D. (*n* = 5 for each group). Note that significantly more fibrosis is induced in mutant livers compared to controls (**, *P* < 0.01).

Fig. 2. Significantly elevated myofibroblast activity in Fn-null livers at 17 weeks of CCl_4 treatment.
(**A**) Left panels: Expression of αSMA (in red) shown by immunofluorescence staining at 0 (untreated) and 17 weeks of CCl_4 treatment. Bar = 100 μm. Right panel: Quantification of αSMA positive areas at 17 weeks of CCl_4 treatment (large blood vessel-positive areas [b] shown in left panels were subtracted). Data are means ± S.D. (*n* = 4 in each group; **, *P* < 0.01).
(**B**) Left panel: Western blot analysis of myofibroblast marker αSMA protein expression at 17 weeks of CCl_4 treatment. Right panel: Analysis of αSMA intensities. Band intensity was measured by densitometry and normalized to β-actin (loading control). The αSMA expression levels are shown relative to the control value of 100 (percent of control). Data are means ± S.D. (*n* = 3 for control and 4 for null mice; *, *P* < 0.05).
(**C**) Immunostaining for cleaved caspase 3 (caspase 3 in brown; nuclei in blue). Note that no apparent positive cells are visible. Bar = 25 μm.

Fig. 3. Significant hepatic dysfunction and increased liver-tissue stiffness in Fn-null livers.
(**A**) - (**C**) Serum levels of the hepatic biochemical markers total bilirubin (**A**), cholinesterase (**B**), and albumin (**C**) during chronic liver injury. Data are means ± S.D. (*n* = 6 for each group). Note that considerable loss of hepatic functional reserve is demonstrated in mutant livers, as evidenced by significant upregulation of total bilirubin and downregulation of cholinesterase levels (*, *P* < 0.05; **, *P* < 0.01).
(**D**) - (**G**) Analysis of liver tissue stiffness using AFM at 17 weeks of CCl_4 treatment.
(**D**) Elastic modulus in liver tissues. Data are means ± S.D. Note that elastic modulus are significantly higher in mutant livers (*n* [measured areas] = 9 for each group *, *P* < 0.05).
(**E**) Gaussian fit of elastic modulus distribution determined pixel-by-pixel with the Peakforce method in a typical collagen fibril-rich area in each group (2 x 2 μm images were used for this analysis).
(**F, G**) AFM images showing (F) a map of mechanical properties (log of the elastic modulus) and (G) topography (height) of collagen fibrils in control and Fn-null liver at 17 weeks of CCl4 treatment. Note that mutant livers show thinner and more dispersed fibrils.

Fig. 4. Lack of Fn results in elevated accumulation of latent TGF-β complexes and continuous activation of TGF-β during chronic liver injury.
(**A**) Significantly increased accumulation of LAP and LTBP-1, -3 and -4 (in red) in the ECM of mutant livers at 17 weeks of CCl_4 treatment shown by immunofluorescence staining using serial sections (**, *P* < 0.01). Bar = 100 μm.

(**B**) Active TGF-β bioassay at 8 and 17 weeks of CCl_4 treatment. Data are means ± S.D. (n = 6 for each group). Note that mutant livers show significantly elevated local TGF-β activity at both time points (*, $P < 0.05$; **, $P < 0.01$).
(**C**) Left panels: Immunostaining for pSmad2/3. Sections were counterstained with hematoxylin. Bar = 25 μm. Right panel: Analysis of pSmad2/3-positive cells. Data are means ± S.D. (n = 10 in each group). Note that the number of nuclear pSmad2/3-positive (in brown) non-parenchymal cells (NPCs; red arrowheads) in mutant livers is significantly higher than controls at 17 weeks of CCl_4 treatment (**, $P < 0.01$). For comparison, hepatocyte nuclei (~two- to three-hold larger than those in non-parenchymal cells) are indicated (black arrows).
(**D**) Left panels: Double immunohistochemical staining for pSmad2/3 (in purple/blue) and αSMA (in brown). Note that the nuclear pSmad2/3-positive cells express myofibroblast marker αSMA in their cytoplasms (black arrowheads). Bar = 25 μm. Right panel: Analysis of pSmad2/3 and αSMA double-positive myofibroblasts. Data are means ± S.D. (n = 10 in each group; **, $P < 0.01$).

Fig. 5. Fn-null livers accumulate more extensive and disorganized collagen fibril networks at 17 weeks of CCl_4 treatment.
(**A**) Upper panels: Deposition of type III and type I collagens at 0 (untreated) and 17 weeks of CCl_4 treatment by immunofluorescent staining. Depositions at 17 weeks are shown using serial sections. Bar = 100 μm. Lower panels: Quantification of positive areas at 17 weeks of CCl_4 treatment. Data are means ± S.D. (n = 4 for each group). Note that deposition of type III and type I collagen is significantly increased in mutant livers compared to controls at 17 weeks of CCl_4 treatment (**, $P < 0.01$).
(**B**) Real-time PCR analysis of *Col1a1* mRNA levels. Relative mRNA expression levels are shown relative to the control value of 1. Data are means ± S.D. (n = 5 for each group). Note that collagen mRNA levels in mutant livers are significantly upregulated (*, $P < 0.05$).
(**C**) - (**E**) Analysis of assembled fibrils using polarized microscopy.
(**C**) Immunofluorescent staining for type I collagen (first upper 2 panels), and representative images of retardance and orientation by Sirius Red-stained serial sections (second and third 2 panels, respectively). The level of retardation is denoted by a pixel color, as indicated by the color legend (from purple [the lowest] to red [the highest]). Note that the maximum magnitude of retardance (red color) is identical in the control and mutant liver. Bars = 25 μm.
(**D**) Representative distribution patterns of fibril bundle orientation in the control and mutant livers. The x-axis represents the orientation angle. This is divided into 10° increments and 0° corresponds to the mean orientation of distributions. The y-axis shows the percentage of fibril bundles within 10° orientation angle range. Note that orientation of fibril bundles in mutant livers is less aligned and more disorganized compared to controls. AD, angular deviation.
(**E**) The average angular deviation of orientation distributions. Data are means ± S.D. Note that angular deviation is significantly larger in mutant livers (**, $P < 0.01$).
(**F**) Real-time PCR analysis of *MMP8 and MMP13* mRNA levels. Relative mRNA expression levels are shown relative to the control value of 1. Data are means ± S.D. (n = 5 for each group). Note that the expression levels are not significantly different.

Fig. 6. Contribution of type V collagen to advanced chronic liver injury and collagen fibril ultrastructure at 17 weeks of CCl_4 treatment.
(**A**) Significantly increased deposition and assembly of type V collagen in mutant livers shown by immunofluorescence staining using serial sections (type V collagen in green; type I collagen in red; Fn in red; DAPI [cell nuclei] in blue) (n = 4 for each group; **, $P < 0.01$). Bar = 50 μm.
(**B**) Real-time PCR analysis of *Col5a1* mRNA levels. Relative mRNA expression levels are shown relative to the control value of 1.0. Data are means ± S.D. (n = 4 for each group). Note that expression levels in mutant livers are ~1.5-fold increased but not significantly different.
(**C**) - (**F**) Ultrastructural analysis of collagen fibrils using TEM.
(**C**) Electron micrographs of longitudinal (upper panel) and transverse (lower panel) sections. Bar = 100 nm.
(**D**) Left panel: The average diameter of collagen fibrils (1,500 fibrils for each group: 375 fibrils per animal, n = 4, were calculated). Note that the average fibril diameter is identical between control and mutant livers. Right panel: Morphometric analysis of collagen fibril diameter (1,500 fibrils for each group: 375 fibrils per animal, n = 4, were

calculated). Note the ~33% increase in the thinner (30-40 nm diameter) and the ~21% decrease in the number of thicker (50-60 nm diameter) collagen fibril-subpopulations evident in mutant livers.
(**E**) Collagen fibril number. Data are means ± S.D. Note that the fibril number is significantly higher in mutant livers (*n* [measured areas] = 18 for each group **, $P < 0.01$).
(**F**) Hydroxyproline contents. Data are means ± S.D. (*n* = 4 for each group). Note that net hepatic collagen content in mutant livers is significantly increased (*, $P < 0.05$).

Fig. 7. Elevated LOX expression level in Fn-null liver at 17 weeks of CCl_4 treatment and its mechanism.
(**A**) Real-time PCR analysis of *LOX and LOXL1-4* mRNA levels in control and mutant livers. Relative mRNA expression levels are shown relative to the control value of 1. Error bars represent standard deviation (*n* = 4 for each group; *, $P < 0.05$; **, $P < 0.01$).
(**B**) Left panels: Western blot analysis of LOX in Fn-null and its parental hepatic stellate cell (HSC) lines with or without treatment of 2 pM TGF-β1 *in vitro*. Aorta tissue lysates from adult wild-type mice were used as a positive control. Right panel: Analysis of induction levels of active LOX in response to TGF-β1 (fold increase). Band intensity was measured by densitometry and normalized to HSC70 (loading control). Data are from three independent experiments. **, $P < 0.01$.
(**C**) Left Panels: Double immunofluorescence staining for LOX (in green) and DAPI (in blue) in Fn-null hepatic stellate cells (HSC) cultured for 18 h with or without 2 pM TGF-β1 treatment. Bar = 25 μm. Right panel: The effect of Smad3 inhibitor SIS3, PI3-kinase inhibitor LY294002, p38 MAP kinase inhibitor PD169316, JNK inhibitor 420119, and MEK1/2 inhibitor PD98059 on TGF-β1 induced LOX expression in Fn-null hepatic stellate cells. Data are means ± S.D. **, $P < 0.01$.

Fig. 8. Structural and mechanical integrity of formed collagen fibril networks in Fn-null hepatic stellate cells.
(**A**) Elastic modulus of collagen fibrils in Fn-null hepatic stellate cells without treatment (Ntx) or with TGF-β1 or TGF-β1 plus 200 μM BAPN, and parental (control) cells without treatment cultured for 7 days. Data are means ± S.D. (*n* [measured areas] = 7 for Fn-null cells; 6 for parental cells. **, $P < 0.01$). #, Fn-null stellate cells do not form collagen fibril network in culture without treatment (26).
(**B**) Immunofluorescence staining for type I collagen (in red) (upper panels) and images showing a peak force error by AFM (lower panels) in Fn-null hepatic stellate cells (HSC) cultured for 7 days with TGF-β1 or TGF-β1 plus 200 μM BAPN. Bar in fluorescence staining = 25 μm. Note that BAPN treatment results in the disruption of longitudinal collagen bundle formation.
(**C**) Elastic modulus of collagen fibrils in Fn-null hepatic stellate cells with 10 μg/ml plasma Fn and parental (control) cells cultured for 7 days. Data are means ± S.D. (*n* [measured areas] = 6 for each group). n.s., not significantly different.

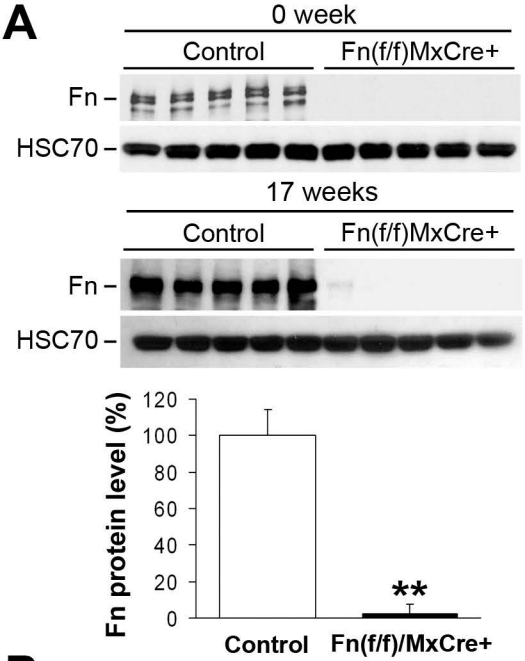
A
0 week
Control
Fn(f/f)MxCre+
Fn
HSC70
17 weeks
Control
Fn(f/f)MxCre+
Fn
HSC70
Fn protein level (%)
120
100
80
60
40
20
0
**
Control
Fn(f/f)/MxCre+

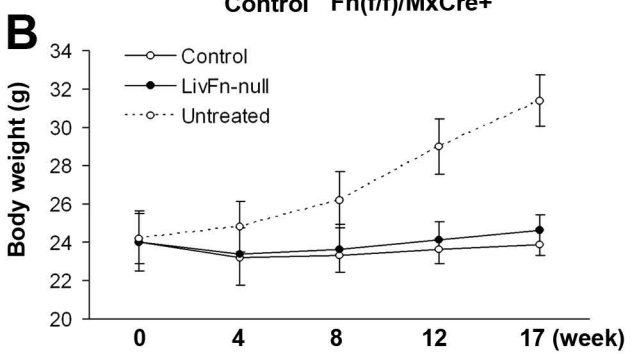
B
Body weight (g)
34
32
30
28
26
24
22
20
Control
LivFn-null
Untreated
0
4
8
12
17 (week)

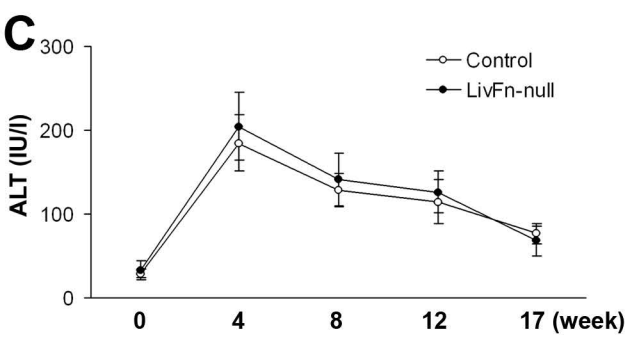
C
ALT (IU/l)
300
200
100
0
Control
LivFn-null
0
4
8
12
17 (week)

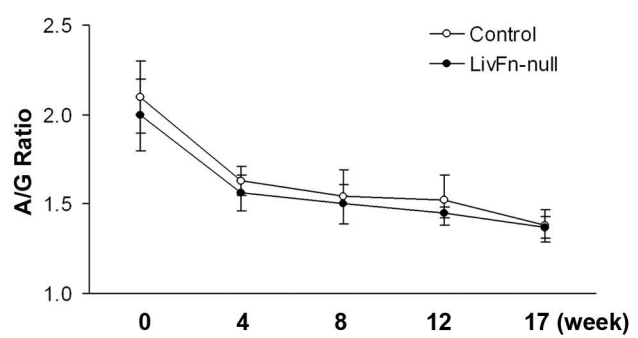
A/G Ratio
2.5
2.0
1.5
1.0
Control
LivFn-null
0
4
8
12
17 (week)

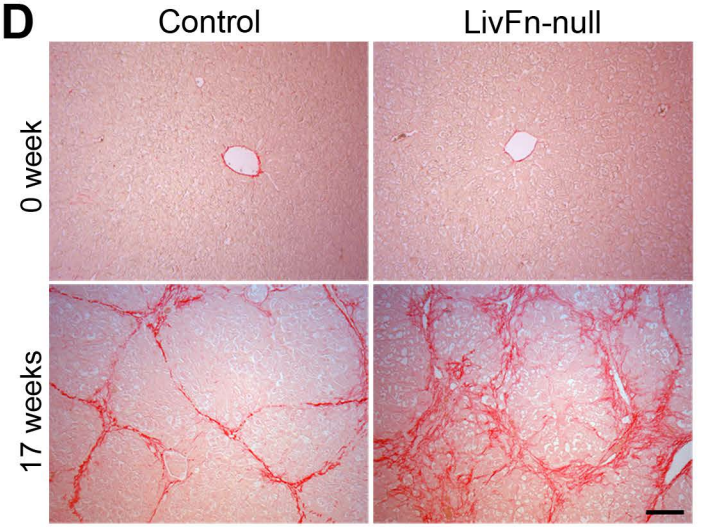
D
Control
LivFn-null
0 week
17 weeks

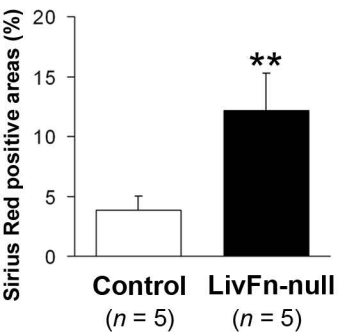
Sirius Red positive areas (%)
20
15
10
5
0
**
Control
(n = 5)
LivFn-null
(n = 5)

Fig. 1

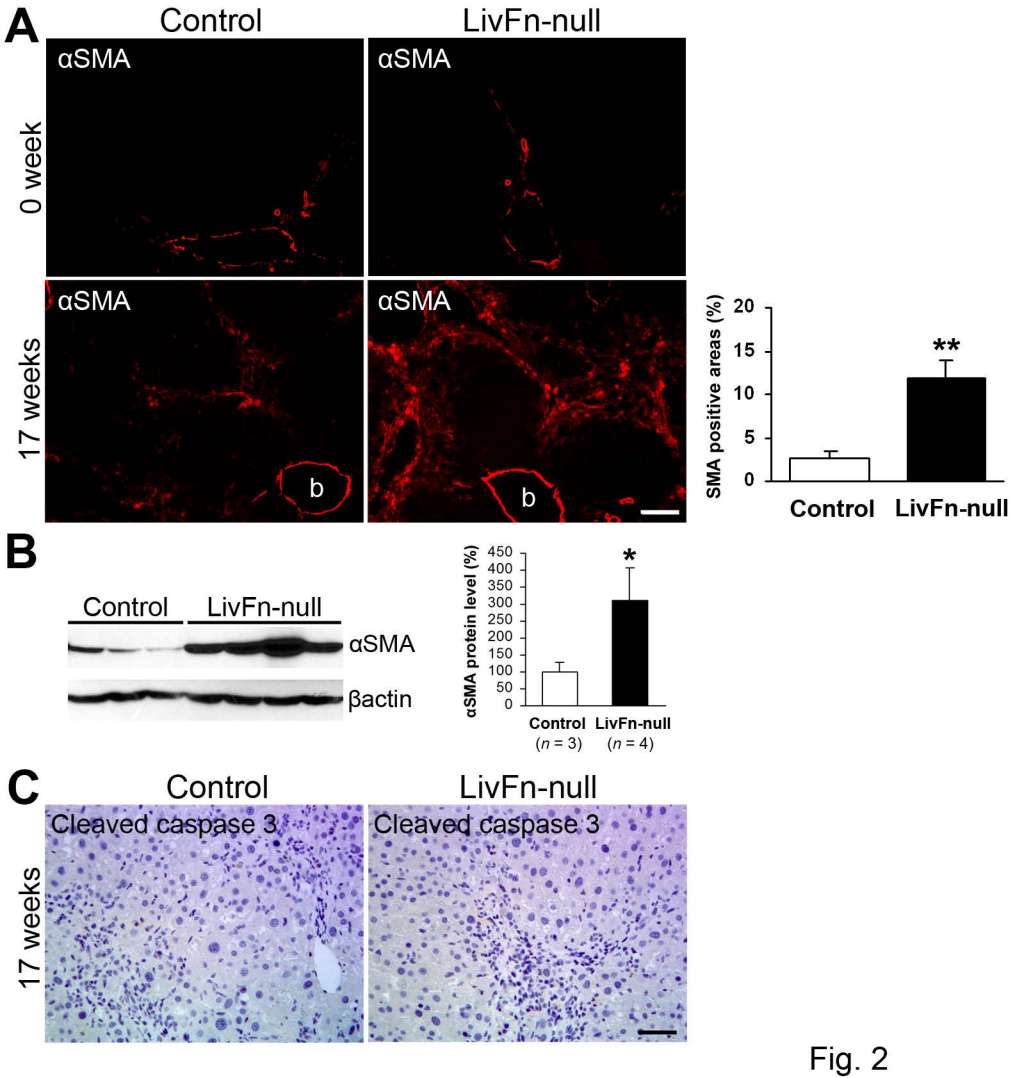
A
Control
LivFn-null
αSMA
αSMA
0 week
αSMA
αSMA
17 weeks
b
b
SMA positive areas (%)
20
15
10
5
0
**
Control
LivFn-null
B
Control
LivFn-null
αSMA
βactin
αSMA protein level (%)
450
400
350
300
250
200
150
100
50
0
*
Control
(n = 3)
LivFn-null
(n = 4)
C
Control
LivFn-null
17 weeks
Cleaved caspase 3
Cleaved caspase 3

Fig. 2

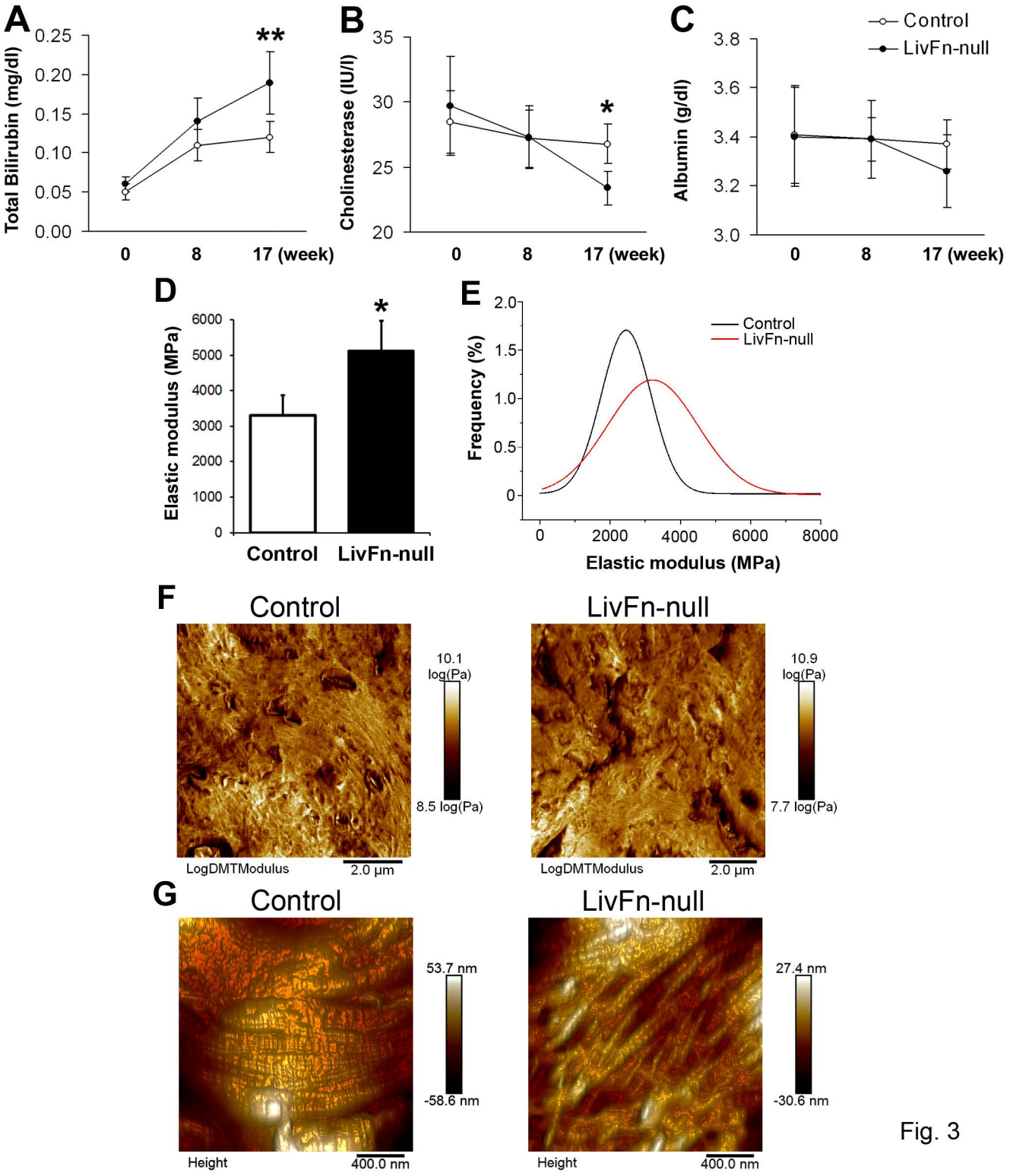
A
Total Bilirubin (mg/dl)
0.25
0.20
0.15
0.10
0.05
0.00
**
0
8
17 (week)
B
Cholinesterase (IU/l)
35
30
25
20
*
0
8
17 (week)
C
Control
LivFn-null
Albumin (g/dl)
3.8
3.6
3.4
3.2
3.0
0
8
17 (week)
D
Elastic modulus (MPa)
6000
5000
4000
3000
2000
1000
0
*
Control
LivFn-null
E
Frequency (%)
2.0
1.5
1.0
0.5
0
Control
LivFn-null
0
2000
4000
6000
8000
Elastic modulus (MPa)
F
Control
10.1
log(Pa)
8.5 log(Pa)
LogDMTModulus
2.0 μm
LivFn-null
10.9
log(Pa)
7.7 log(Pa)
LogDMTModulus
2.0 μm
G
Control
53.7 nm
-58.6 nm
Height
400.0 nm
LivFn-null
27.4 nm
-30.6 nm
Height
400.0 nm

Fig. 3

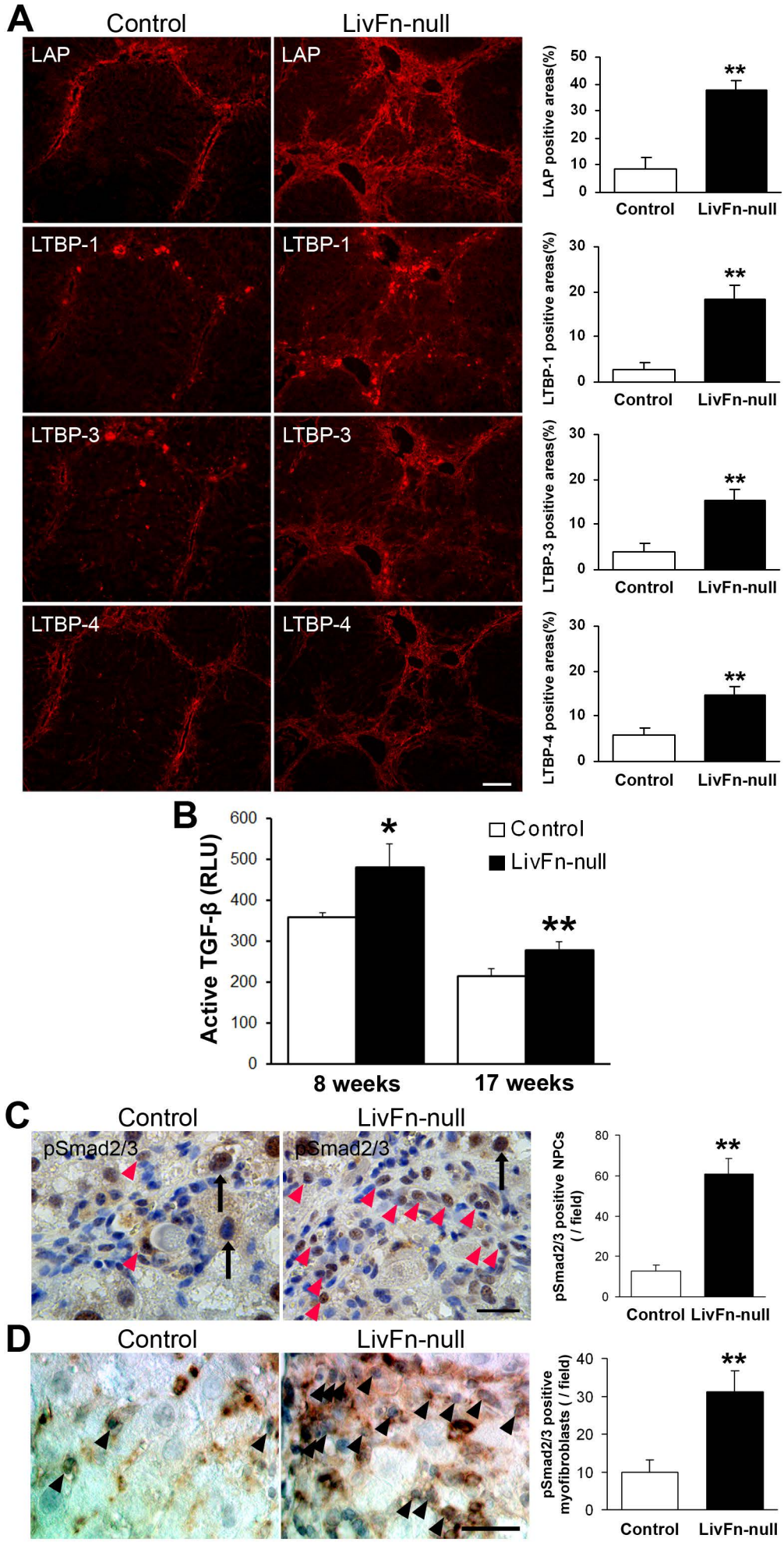
A
Control
LivFn-null
LAP
LAP
LAP positive areas(%)
50
40
30
20
10
0
**
Control
LivFn-null
LTBP-1
LTBP-1
LTBP-1 positive areas(%)
30
20
10
0
**
Control
LivFn-null
LTBP-3
LTBP-3
LTBP-3 positive areas(%)
30
20
10
0
**
Control
LivFn-null
LTBP-4
LTBP-4
LTBP-4 positive areas(%)
30
20
10
0
**
Control
LivFn-null
B
Active TGF-β (RLU)
600
500
400
300
200
100
0
*
**
Control
LivFn-null
8 weeks
17 weeks
C
Control
LivFn-null
pSmad2/3
pSmad2/3
pSmad2/3 positive NPCs (/ field)
80
60
40
20
0
**
Control
LivFn-null
D
Control
LivFn-null
pSmad2/3 positive myofibroblasts (/ field)
40
30
20
10
0
**
Control
LivFn-null

Fig. 4

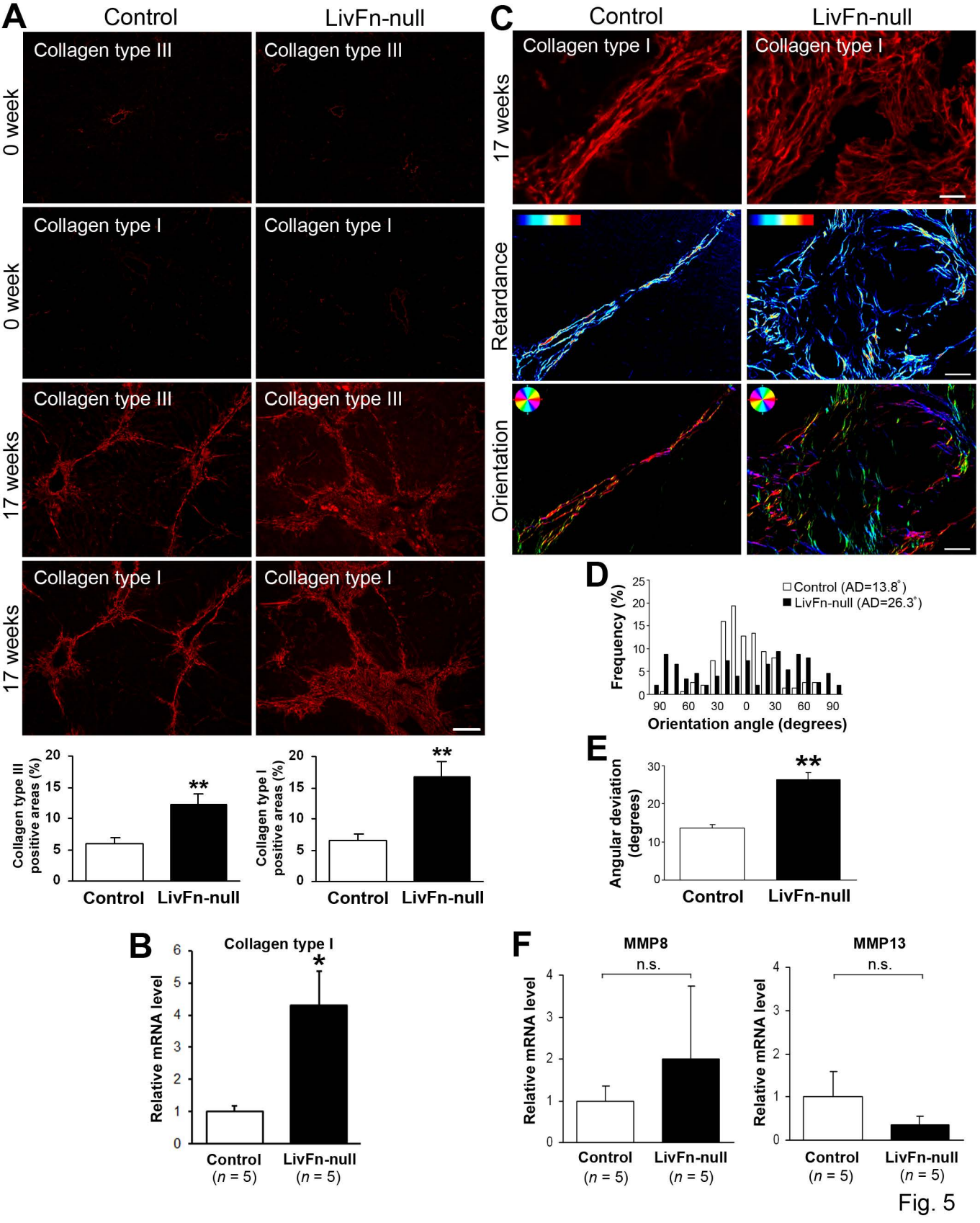
A
Control
LivFn-null
Collagen type III
Collagen type I
0 week
17 weeks
Collagen type III positive areas (%)
Collagen type I positive areas (%)
**
Control
LivFn-null
B
Collagen type I
*
Relative mRNA level
Control (n = 5)
LivFn-null (n = 5)
C
Control
LivFn-null
17 weeks
Retardance
Orientation
D
Control (AD=13.8°)
LivFn-null (AD=26.3°)
Frequency (%)
Orientation angle (degrees)
E
Angular deviation (degrees)
F
MMP8
MMP13
n.s.
Relative mRNA level
Control (n = 5)
LivFn-null (n = 5)

Fig. 5

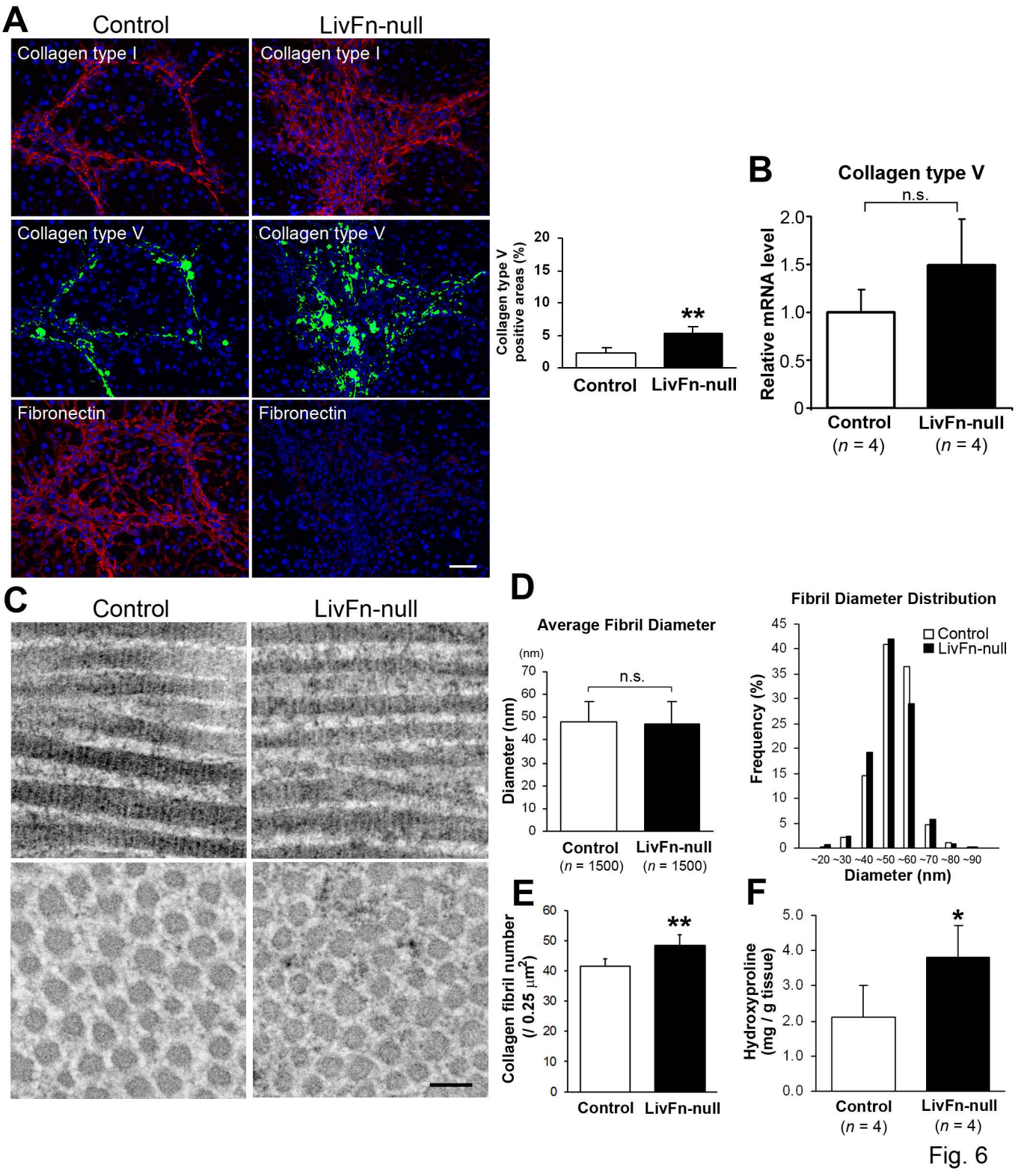
A
Control
LivFn-null
Collagen type I
Collagen type I
Collagen type V
Collagen type V
Fibronectin
Fibronectin
Collagen type V positive areas (%)
20
15
10
5
0
**
Control
LivFn-null
B
Collagen type V
n.s.
Relative mRNA level
2.0
1.5
1.0
0.5
0
Control
(n = 4)
LivFn-null
(n = 4)
C
Control
LivFn-null
D
Average Fibril Diameter
(nm)
70
60
50
40
30
20
10
0
Diameter (nm)
n.s.
Control
(n = 1500)
LivFn-null
(n = 1500)
Fibril Diameter Distribution
Control
LivFn-null
Frequency (%)
45
40
35
30
25
20
15
10
5
0
~20 ~30 ~40 ~50 ~60 ~70 ~80 ~90
Diameter (nm)
E
Collagen fibril number
(/ 0.25 μm2)
60
50
40
30
20
10
0
**
Control
LivFn-null
F
Hydroxyproline
(mg / g tissue)
5.0
4.0
3.0
2.0
1.0
0.0
*
Control
(n = 4)
LivFn-null
(n = 4)

Fig. 6

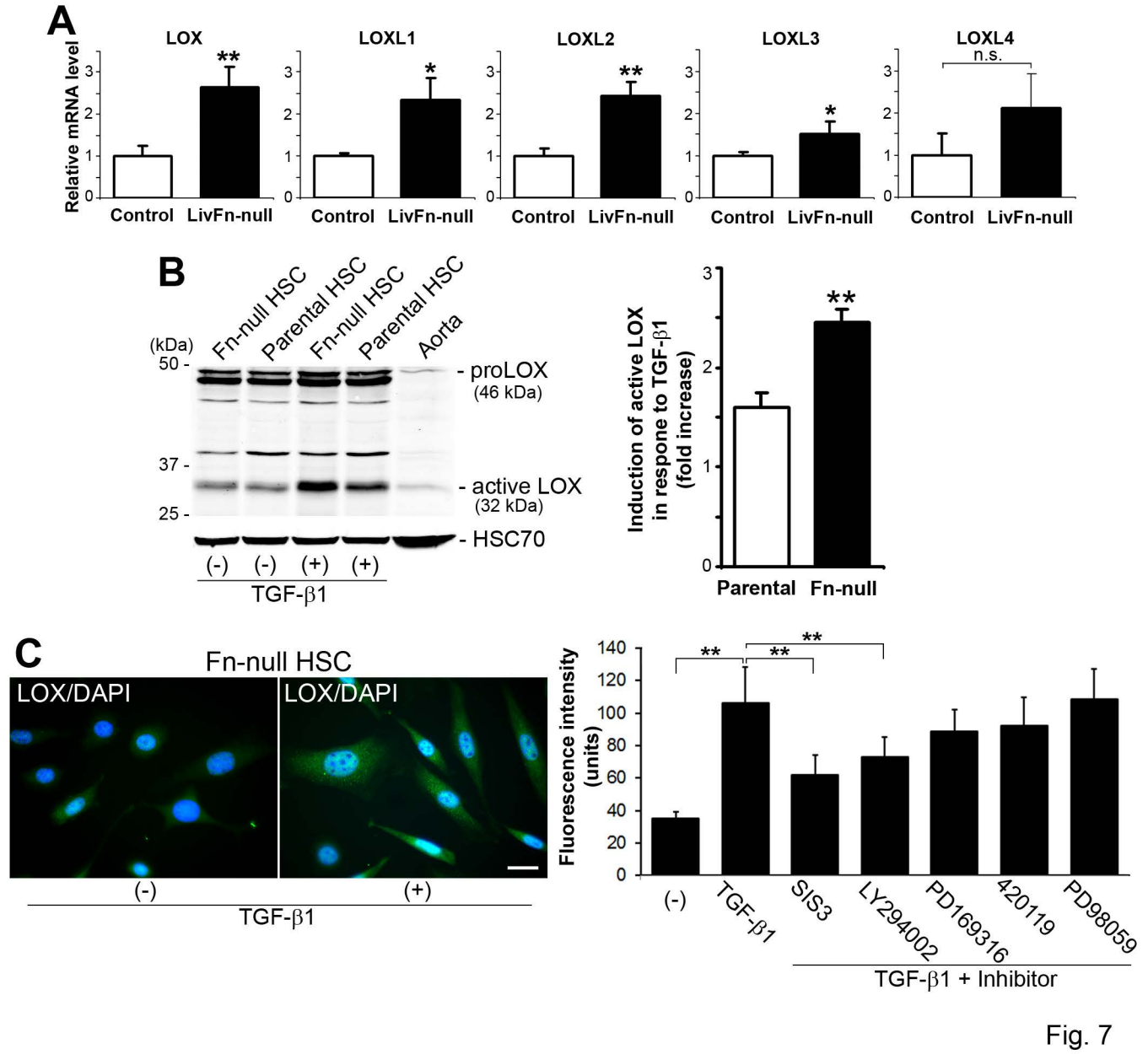
A
LOX
LOXL1
LOXL2
LOXL3
LOXL4
n.s.
Relative mRNA level
Control
LivFn-null
B
Fn-null HSC
Parental HSC
Fn-null HSC
Parental HSC
Aorta
(kDa)
50 -
37 -
25 -
- proLOX
(46 kDa)
- active LOX
(32 kDa)
- HSC70
(-) (-) (+) (+)
TGF-β1
Induction of active LOX
in respone to TGF-β1
(fold increase)
Parental
Fn-null
C
Fn-null HSC
LOX/DAPI
LOX/DAPI
(-)
(+)
TGF-β1
Fluorescence intensity
(units)
(-)
TGF-β1
SIS3
LY294002
PD169316
420119
PD98059
TGF-β1 + Inhibitor

Fig. 7

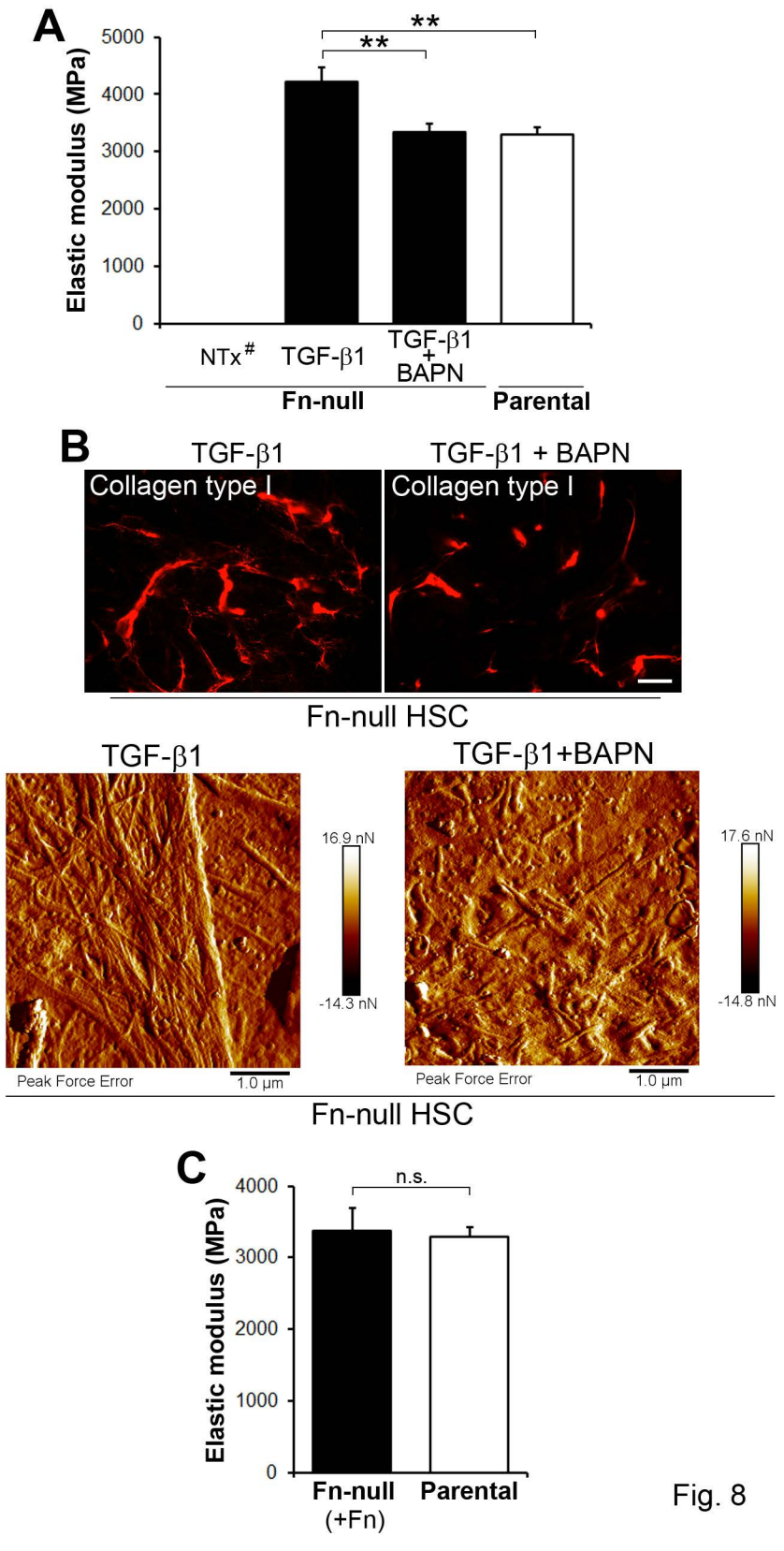
A
Elastic modulus (MPa)
5000
4000
3000
2000
1000
0
**
**
NTx#
TGF-β1
TGF-β1 + BAPN
Fn-null
Parental
B
TGF-β1
TGF-β1 + BAPN
Collagen type I
Collagen type I
Fn-null HSC
TGF-β1
TGF-β1+BAPN
16.9 nN
-14.3 nN
17.6 nN
-14.8 nN
Peak Force Error
1.0 μm
Peak Force Error
1.0 μm
Fn-null HSC
C
Elastic modulus (MPa)
4000
3000
2000
1000
0
n.s.
Fn-null
(+Fn)
Parental

Fig. 8

Glycobiology and Extracellular Matrices:

Molecular mechanism responsible for fibronectin-controlled alterations in tissue stiffness in advanced chronic liver fibrogenesis

Ayumi Iwasaki, Keiko Sakai, Kei Moriya, Takako Sasaki, Douglas R. Keene, Riaz Akhtar, Takayoshi Miyazono, Satoshi Yasumura, Masatoshi Watanabe, Shin Morishita and Takao Sakai

J. Biol. Chem. *published online November 9, 2015*